1   **Novel Role of UHRF1 in DNA methylation-mediated repression of latent HIV-1**

2

3   Roxane Verdikt[1,*], Sophie Bouchat[1,*], Alexander O. Pasternak[2], Lorena Nestola[1], Gilles Darcis[3],

4   Véronique Avettand-Fenoel[4,5,6,7], Caroline Vanhulle[1], Amina Aït-Ammar[1], Maryam Bendoumou[1],

5   Estelle Plant[1], Valentin Le Douce[8], Nadège Delacourt[1], Aurelija Cicilionytė[2], Coca Necsoi[9], Francis

6   Corazza[10], Caroline Pereira Bittencourt Passaes[11], Christian Schwartz[12,13], Martin Bizet[14], François

7   Fuks[14], Asier Sáez-Cirión[11], Christine Rouzioux[4], Stéphane De Wit[9], Ben Berkhout[2], Virginie Gautier[8],

8   Olivier Rohr[11,12,†] and Carine Van Lint[1, †, #]

9

10   [1] Service of Molecular Virology, Department of Molecular Biology (DBM), Université Libre de

11   Bruxelles (ULB), 6041 Gosselies, Belgium

12   [2] Amsterdam UMC, University of Amsterdam, Laboratory of Experimental Virology, Department of

13   Medical Microbiology, 1105 AZ Amsterdam, The Netherlands

14   [3] Infectious Diseases Department, Liège University Hospital, 4000 Liège, Belgium

15   [4] AP-HP, Hôpital Necker-Enfants-Malades, Service de Microbiologie clinique, 75015 Paris, France

16   [5] Université Paris Descartes, Sorbonne Paris Cité, Faculté de Médecine, Paris, France

17   [6] INSERM, U1016, Institut Cochin, Paris, France

18   [7] CNRS, UMR8104, Paris, France

19   [8] Centre for Research in Infectious Diseases, University College Dublin, Dublin 4, Ireland

20   [9] Service des Maladies Infectieuses, CHU St-Pierre, Université Libre de Bruxelles (ULB), 1000

21   Brussels, Belgium

22   [10] Laboratory of Immunology, IRISLab, CHU Brugmann, Université Libre de Bruxelles (ULB), 1020

23   Brussels, Belgium

24   [11] Institut Pasteur, Unité HIV, Inflammation et Persistance, Départements de Virologie et Immunologie,

25   75015 Paris, France

26   [12] Université de Strasbourg, laboratoire DHPI EA7292, Schiltigheim, France

27   [13] IUT Louis Pasteur, Université de Strasbourg, Schiltigheim, France

28   [14] Laboratory of Cancer Epigenetics, Faculty of Medicine, ULB-Cancer Research Center (U-CRC),

29   Université Libre de Bruxelles (ULB), 1070 Brussels, Belgium

30

31   [*,†] These authors contributed equally to this work.

32   [#] Corresponding Author: cvlint@ulb.ac.be

33

34 **ABSTRACT**

35 The multiplicity, heterogeneity and dynamic nature of HIV-1 latency mechanisms are reflected in the

36 current lack of functional cure for HIV-1 and in the various reported *ex vivo* potencies of latency-

37 reversing agents. Here, we investigated the molecular mechanisms underlying the potency of the DNA

38 methylation inhibitor 5-aza-2'-deoxycytidine (5-AzadC) in HIV-1 latency reversal. Doing so, we

39 uncovered specific demethylation CpG signatures induced by 5-AzadC in the HIV-1 promoter. By

40 analyzing the binding modalities to these CpG, we revealed the recruitment of the epigenetic integrator

41 UHRF1 to the HIV-1 promoter. We further demonstrated the role of UHRF1 in DNA methylation-

42 mediated silencing of the latent HIV-1 promoter. As a proof-of-concept to this molecular

43 characterization, we showed that pharmacological downregulation of UHRF1 in *ex vivo* HIV$^+$ patient

44 cell cultures resulted in potent reactivation of latent HIV-1. Together, we identify UHRF1 as a novel

45 actor in HIV-1 gene silencing and highlight that it constitutes a new molecular target for HIV-1 curative

46 strategies.

47

48 **KEYWORDS**

49 HIV-1 latency, DNA methylation, reactivation, UHRF1, EGCG.

50

INTRODUCTION

51
52   Combination antiretroviral therapy (cART) is the only therapeutic option available for HIV-
53 1infected individuals. If cART is efficient in suppressing viral replication and in prolonging the lifespan
54 of infected individuals, the persistence of transcriptionally-silent proviruses, particularly in latently-
55 infected resting memory CD4$^+$ T cells, still prevents HIV-1 eradication (1–3). As such, much effort has
56 been put in understanding the multiple molecular factors involved in viral latency to develop new anti-
57 HIV therapeutic strategies. One such strategy relies on the use of latency-reversing agents (LRAs) that
58 target repressors of HIV-1 gene expression, thereby inducing a controlled activation of latent reservoirs
59 (4, 5).

60   The multifactorial process of HIV-1 silencing during latency is controlled in part by the viral
61 transactivator Tat and by cellular transcription factors (TFs) binding sites (TFBS) present in the viral
62 promoter, located in the 5' long terminal repeat (5'LTR)(6). In addition, epigenetic processes controlling
63 the chromatin architecture of latent HIV-1 proviruses play key roles in viral transcriptional silencing (7,
64 8). Two CpG islands (CGIs) present in the 5'LTR region and surrounding the transcription start site
65 have been reported to be hypermethylated in latently-infected model T-cell lines (Fig. 1A), thus
66 participating in the 5'LTR heterochromatinization during latency (9–11). Methylation of the HIV-1
67 promoter in patient cells has been reported in some studies (9, 10, 12) but other reports denied the
68 implication of 5'LTR methylation *ex vivo* (13–15). To explain these contradictory results, recent studies
69 proposed that patients clinical characteristics, such as duration of the infection (12) and duration of the
70 antiretroviral treatment (16, 17), might influence the accumulation of DNA methylation in the 5'LTR.
71 In agreement with these heterogeneous profiles of DNA methylation on the HIV-1 promoter *ex vivo*, we
72 have previously shown that latency reversal with the DNA methylation inhibitor 5-aza-2'-deoxycytidine
73 (5-AzadC or decitabine) is associated with patient-specific qualitative and quantitative variations in
74 HIV-1 reactivation from latency (18).

75   Here, we studied the molecular basis to 5-AzadC reactivation potency of HIV-1 latency reversal
76 in terms of proviral DNA demethylation. By highlighting the presence of specific epigenetic signatures
77 in the HIV-1 promoter following 5-AzadC reactivation, we uncovered the role of the epigenetic
78 integrator UHRF1 (Ubiquitin-like with PHD and RING finger domain 1) in the control of HIV-1 latency.
79 As a proof-of-concept, we showed evidence that pharmacological downregulation of UHRF1 constitutes
80 a novel therapeutic approach for anti-HIV-1 curative strategies.

81   **RESULTS**

82   **5-AzadC treatment provokes specific demethylation signatures in the HIV-1 5'LTR.**

83   We first analyzed how variations in 5-AzadC reactivation potency translated at the DNA

84   methylation level in the HIV-1 promoter CGIs. To do so, we mock-treated or treated four clones of the

85   CD4$^+$ T-lymphoid J-Lat cell line model for HIV-1 latency with 5-AzadC. First, quantification of the

86   viral progeny particles capsid protein p24^{Gag} in the treated culture supernatants by ELISA confirmed the

87   variation in 5-AzadC reactivation potency *in vitro* (Fig. 1B/D/F/H, , indicating a 10.6 fold, a 2.9 fold, a

88   2.4 fold and a 12.1 fold reactivation, for J-Lat 6.3, J-Lat 8.4, J-Lat 9.2 and J-Lat 15.4 cells, respectively).

89   We next assessed the methylation status of the two promoter CGIs termed 5'LTR and NCR CGIs (from

90   nt -455 to nt 179 and from nt 183 to nt 470, respectively, where nt+1 is at the U3/R junction in the

91   5'LTR, Fig. 1A) and of a control intragenic CGI located within *rev* termed ETR CGI (nt 7924 to nt

92   8196, Fig. 1A)(11). Because the two viral LTRs have identical sequences and because we wanted to

93   specifically obtain the methylation profile of the 5'LTR, both 5'LTR and NCR CGIs were analyzed in

94   a single amplicon. We confirmed that promoter CGIs were hypermethylated to similar levels in the four

95   J-Lat clones in mock-treated conditions (Fig. 1C/E/G/I, 92.19%, 92.44%, 89.06% and 91.4% of 5mC,

96   respectively, for J-Lat 6.3, J-Lat 8.4, J-Lat 9.2 and J-Lat 15.4 cells), consistent with previous

97   observations (9, 10). Treatment with 5-AzadC provoked a global demethylation in the two promoter

98   CGIs, though to various extents in each J-Lat clone allowing the following ranking: J-Lat 6.3 cells

99   (29.17% of 5-AzadC-induced demethylation) > J-Lat 15.4 cells (24.99%) > J-Lat 8.4 cells (19.36%) >

100   J-Lat 9.2 cells (5.21%) (Fig. 1, respective p-values of 0.0057; 0.0020; 0.0085; 0.0142; unpaired T test).

101   This ranking was similar to the one we observed with the fold reactivation levels of HIV-1 production,

102   indicating that 5-AzadC reactivation is dependent on specific demethylation of sites in the HIV-1

103   promoter but with a heterogeneous profile. As a control, treatment with 5-AzadC did not alter the

104   methylation profile of the HIV-1 ETR CGI in J-Lat 6.3 cells, J-Lat 8.4 cells and J-Lat 15.4 cells (Fig.

105   1C/E/I, respectively). Of note and in agreement with lower basal promoter CGIs methylation level, 5-

106   AzadC reactivation fold in HIV-1 production was the lowest in the J-Lat 9.2 clone (Fig. 1F), in which

107   the ETR CGI was also demethylated following 5-AzadC treatment, suggesting a non-specific action for

108   5-AzadC on the HIV-1 promoter in this clone (Fig. 1G).

109   To tease out for specific regulatory mechanisms underlying the heterogeneity of 5-AzadC

110   reactivation potency, we next mapped the probability of demethylation following 5-AzadC treatment at

111   individual CpG positions in promoter CGIs. This probabilistic analysis highlighted that some CpGs were

112   more prone to 5-AzadC-induced demethylation (Fig. S1 and Methods section). The most statistically

113   significant 5-AzadC-induced differentially-demethylated positions (termed "DDMPs") are listed in

114   Table 1. Despite some similarities, the position of statistically significant DDMPs varied among J-Lat

115   clones, illustrating the heterogeneity of the 5-AzadC-induced mechanisms of HIV-1 reactivation from

116   latency recapitulated by the clones. Some DDMPS were present in sequences giving rise to viral RNA

117   features (PBS or the packaging sequence signal ψ), suggesting a potential link between DNA

4

118   methylation deposition and RNA structuration (Table 1). Importantly, several DDMPs were located

119   within TFBS involved in HIV-1 transcriptional regulation, in the cAMP-Responsive Element

120   (CRE)(19), NF-κB binding sites (19), Sp1 binding sites (20, 21), and interferon-stimulated response

121   element (21) (highlighted in Figure 1A and Table 1).

122   **Methylation of HIV-1 DDMP5 allows the recruitment of UHRF1.**

123   We next focused on the DDMP identified in J-Lat 8.4 cells and located at nucleotide positions

124   -120 to -119 in the HIV-1 promoter, referred to as DDMP5 hereafter (Table 1, Figure 1). Indeed,

125   DDMP5 presented the highest demethylation probability and was the most statistically significant

126   among all identified DDMPs within TFBS in all clones (Table 1, 5-AzadC-induced demethylation

127   probability=0.64 and p-value=0.005, Fisher's exact test). DDMP5 is located within a known HIV-1

128   promoter CRE (19). Since genome-wide studies have shown that DNA methylation generally affects

129   negatively the binding of CRE factors to their cognate sites (22), we hypothesized that DDMP5

130   methylation would prevent the binding of cognate transcriptional activators to the HIV-1 promoter CRE.

131   We thus performed electrophoretic mobility shift assays (EMSAs) using radiolabeled double-

132   stranded oligonucleotide probes containing the HIV-1$_{NL4.3}$ DDMP5 sequence in an unmethylated

133   ("DDMP5") or in a methylated ("DDMP5-me") form. These assays showed that the unmethylated

134   DDMP5 probe was bound by a single retarded DNA-protein complex, termed C1 (Fig. 2A). In supershift

135   experiments, addition of antibodies raised against CREB and CREM provoked a decreased in the

136   complex C1 formation (Fig. 2A, lane 4 and lane 5, indicated by an asterisk), whereas addition of the

137   IgG control or of antibodies raised against ATF1 did not affect complex formation (Fig. 2A, lane 3 and

138   lane 6, respectively), demonstrating that the C1 complex contains both CREB and CREM proteins.

139   Furthermore, the C1 complex was still observed when the DDMP5 probe was methylated (Fig. 2A, lane

140   8) and supershift experiments showed that CREB and CREM factors could bind to the same extent to

141   the methylated and unmethylated probes (Fig. 2A, lane 10 and lane 11, respectively). We further

142   confirmed that the binding of proteins in the C1 complex was independent of the DDMP5 methylation

143   status, since molar excesses of both methylated and unmethylated DDMP5 competed out complex C1

144   formation (Fig. S2A, compare lanes 3-5 with lanes 11-13 and Fig. S2B). Together, these data indicate

145   that DNA methylation in the HIV-1 promoter CRE site neither prevented nor decreased the binding of

146   its cognate factors. The discrepancy between our results and the reported genome-wide DNA

147   methylation-induced inhibition of CRE factors binding (22) could be explained by sequence differences

148   in this TFBS motif (Fig. 2A).

149   Interestingly, we observed by EMSAs the formation of an additional retarded complex, termed

150   C2, with the methylated HIV-1 DDMP5 probe (Fig. 2A, lanes 8 to 12). We found that the C2 complex

151   was formed only when the DDMP5 probe was methylated and was competed out only by methylated

152   DDMP5 oligonucleotides (Fig. S2A, lanes 7-9). Furthermore, formation of the C2 complex was not

153   competed out by molar excesses of the methylated consensus for methyl-binding domain (MBD)

154   proteins, or of the methylated consensus for Sp1, indicating that the proteins contained within the C2

155 complex were specific to the methylated HIV-1 DDMP5, and not to any 5mC-containing sequence (Fig.

156 S2C). Because our *in vitro* experiments showed that, rather than preventing the binding of transcriptional

157 activators, DDMP5 methylation allowed the binding of methylCpG-recognizing proteins to the HIV-1

158 promoter, we investigated the nature of the proteins present in the C2 complex. To do so, we performed

159 additional supershift experiments, using antibodies raised against proteins known to bind

160 methylcytosines (MBD2, MBD4, MeCP2, Kaiso, UHRF1 and RBP-JK)(23, 24). Addition of an

161 antibody raised against UHRF1, but not against the other proteins, altered the formation of the C2

162 complex, concomitantly with the appearance of a supershifted complex of lower mobility (Fig. 2B, lane

163 9, indicated with an asterisk), while addition of IgG did not affect complex C2 formation (Fig. 2B, lane

164 5). These results thus indicated that the C2 complex contained UHRF1 that bound *in vitro* to the

165 methylated HIV-1 DDMP5.

166 To demonstrate *in vivo*, within the context of chromatin, the relevance of UHRF1 binding to the

167 HIV-1 promoter, we performed chromatin immunoprecipitation (ChIP) assays in J-Lat 8.4 cells. Using

168 primers hybridizing specifically to the HIV-1 5'LTR, in the Nuc-1 region, we showed that UHRF1 was

169 recruited to the latent promoter in J-Lat 8.4 cells (Fig. 2C, 20.75-fold recruitment). Furthermore, 5-

170 AzadC-induced demethylation, allowing DNA demethylation of DDMP5 (Fig. 1E), was accompanied

171 by a statistically significant decrease in UHRF1 recruitment to the viral promoter (Fig. 2C, 22.9-fold

172 decrease, p=0.01, unpaired T test). As a control, we quantified *UHRF1* mRNA and protein levels in J-

173 Lat 8.4 cells in response to 5-AzadC (Fig. S3A and Fig. S3B, respectively), and showed that 5-AzadC

174 did not alter UHRF1 expression, thus demonstrating a direct link between UHRF1 decreased recruitment

175 to the HIV-1 promoter and its 5-AzadC-induced demethylation. Despite the fact that DDMP5 had been

176 identified in the J-Lat 8.4 clone, we next assessed whether UHRF1 *in vivo* recruitment to the HIV-1

177 5'LTR was a common feature of HIV-1 latency. These additional ChIP experiments showed that

178 UHRF1 was also recruited to the latent viral promoter in the J-Lat 6.3 and J-Lat 15.4 cells, albeit to

179 lower levels than in the J-Lat 8.4 cells (Fig. 2D, 5.35-fold and 3.75-fold recruitment, respectively). To

180 determine how UHRF1 recruitment modalities correlated to DDMP5 methylation status in the 5'LTR,

181 we plotted UHRF1 fold recruitment from our ChIP results to DDMP5 methylation level in latent

182 conditions in all four J-Lat clones. This showed that UHRF1 *in vivo* recruitment followed the status of

183 the DDMP5 methylation status in the four clones analyzed, with a trend towards higher recruitment of

184 UHRF1 to more methylated DDMP5 (Fig. 2E). For instance, J-Lat 9.2 cells, in which DDMP5 was

185 already largely unmethylated in basal conditions (Fig. 1G, 9 clones unmethylated on 12) showed weak

186 *in vivo* UHRF1 recruitment to the HIV-1 promoter (Fig. 2E). Of note, the lack of significant correlation

187 between UHRF1 *in vivo* recruitment and the DDMP5 methylation status in the 5'LTR can be explained

188 by its independent recruitment to the viral promoter through other epigenetic marks, thanks to UHRF1

189 domains for histone methylation or acetylation (25, 26), through interaction with other epigenetic

190 enzymes (27, 28) or through direct recognition of binding motifs in the 5'LTR (29).

191   Taken together, our results demonstrated that the 5'LTR DDMP5 position corresponds to an *in*

192   *vitro* binding site for UHRF1. We confirmed the *in vivo* recruitment of UHRF1 to the latent HIV-1

193   5'LTR and showed it is proportional to the methylation level of a single CpG residue. Furthermore,

194   reactivation of HIV-1 gene expression following 5-AzadC treatment was accompanied by the

195   demethylation of DDMP5 and by a decreased UHRF1 recruitment to the viral promoter, suggesting a

196   role for UHRF1 in DNA methylation-mediated silencing of HIV-1 gene expression.

UHRF1 transcriptional repression of the HIV-1 promoter is DNA methylation-dependent.

198   To determine the involvement of UHRF1 in the maintenance or establishment of transcriptional

199   silencing at the HIV-1 promoter during latency, we induced the downregulation of endogenous UHRF1

200   by shRNAs. J-Lat 8.4 cells were mock-transduced, or stably transduced with lentiviral vectors

201   expressing the puromycin-resistance gene and containing one out of four different shRNAs targeting

202   UHRF1 mRNA (shUHRF1#1-4) or a control non-targeting shRNA (shNT). UHRF1 knockdown in

203   selected puromycin-resistant clones was confirmed both by western blot analyses and by RT-qPCR (Fig.

204   S4A and S4B, respectively). Because UHRF1 is essential in the cell cycle control and its downregulation

205   is associated with cellular mortality (30, 31), we selected for further analyses one shUHRF1 that did not

206   provoke the most efficient downregulation of UHRF1 but that would, therefore, not be counter-selected

207   (Fig. S4, pLV shUHRF1#4). First, by ChIP experiments, we showed that RNAPII recruitment to the

208   Nuc-1 region of the HIV-1 promoter was statistically higher in UHRF1-depleted J-Lat 8.4 cells than in

209   shNT-transduced cells, consistent with a release of viral transcriptional blocks from latency (Fig. 3A,

210   2.48-fold increase, p=0.008, unpaired T test). Reactivation of HIV-1 gene expression from latency in J-

211   Lat 8.4 cells following UHRF1 knockdown was further studied by quantifying by RT-qPCR initiated

212   (TAR region) and elongated (*tat* region) HIV-1 transcripts (Fig. 3B). A statistically higher number of

213   initiated and elongated transcripts was observed when UHRF1 was knocked down in J-Lat 8.4 cells,

214   compared to the amount measured in shNT-transduced cells (Fig. 3B, 3.29-fold increase, p=0.0011 and

215   1.7-fold, p=0.034, for TAR and *tat*, respectively, unpaired T test). This indicates that the observed

216   increase in RNAPII recruitment was accompanied by an increased transcription initiation and elongation

217   from the HIV-1 promoter. In addition, we observed a statistically significant increase in multiply spliced

218   (MS) HIV-1 RNA (32) in shUHRF1-transduced cells compared to shNT-transduced cells (Fig. 3B, 2.99-

219   fold increase, p=0.0004, unpaired T test). Finally, quantification of p24^{Gag} capsid protein by ELISA in

220   culture supernatants from puromycin-resistant clones showed that UHRF1 knockdown was

221   accompanied by a higher HIV-1 production than the one observed in the shNT-transduced cells (Fig.

222   3C, 4.5-fold increase, p=0.02, unpaired T test). We observed this statistically significant increase in

223   HIV-1 production upon UHRF1 depletion with the four shUHRF1 we used (Fig. S4C), strengthening

224   the specific role of UHRF1 in HIV-1 silencing. Of note, J-Lat 8.4 cells transduction with the control,

225   non-targeting shRNA, also caused reactivation of HIV-1 gene expression and production, though to

226   lower levels than transduction of the shUHRF1, as seen by increased HIV-1 initiating, *gag* and multiply

227   spliced transcripts (Fig. 3B) and increased HIV-1 production (Fig. 3C and Fig. S4C). This was consistent

228   with the use of lentiviral shRNA vectors and was in agreement with a previous report (33). Nevertheless,

229   we observed the reactivation of HIV-1 gene expression and production when shUHRF1-transduced

230   conditions were normalized to shNT-transduced conditions, and *a fortiori*, when normalized to mock-

231   transduced conditions (Fig. 3A-C). Together, these data demonstrated that UHRF1 knockdown enables

232   a full release (i.e. up to the completion of the replication cycle and the production of progeny particles)

233   of the transcriptional blocks from latency in J-Lat 8.4 cells, thereby indicating a role for UHRF1 in the

234   maintenance of HIV-1 latency.

235   Because UHRF1 is an important epigenetic integrator in the heterochromatinization of *cis*-

236   regulatory sequences (25, 34, 35), we next further investigated how UHRF1 knockdown and subsequent

237   reactivation of HIV-1 gene expression translated in terms of DNA methylation modifications on the

238   HIV-1 promoter. UHRF1 knockdown was associated with a statistically significant decrease in global

239   HIV-1 promoter DNA methylation compared to mock-transduced conditions (Fig. 3D), whereas no

240   DNA demethylation was observed on the control ETR CGI. These results thus indicate that UHRF1

241   depletion leads to HIV-1 transcriptional reactivation through specific 5'LTR demethylation. Of note,

242   the demethylation signatures in the HIV-1 promoter CGIs in response to UHRF1 depletion were similar

243   than those in 5-AzadC-treated cells (compare Fig. 3D and Fig. 1E). Indeed, the fifth CpG dinucleotide

244   in the 5'LTR CGI showed a high demethylation probability in response to UHRF1 knockdown (Fig.

245   S4), linking mechanistically UHRF1 with 5-AzadC-induced reactivation in J-Lat 8.4 cells. In addition,

246   shNT transduction that provoked HIV-1 reactivation was also accompanied by global 5'LTR

247   demethylation and by demethylation of DDMP5, further highlighting that the DDMP5 methylation state

248   is functionally linked to the level of HIV-1 gene silencing (Fig. 3D). UHRF1 has been showed to interact

249   with multiple epigenetic enzymes, including DNMT1 (30, 36) and G9a/EHMT2 (27, 28), that are

250   important actors in the HIV-1 promoter heterochromatinization during latency (reviewed in (8)). We

251   thus determined the effect of UHRF1 downregulation on the *in vivo* recruitment of DNMT1 and

252   G9a/EHMT2 to the viral promoter. Following depletion of UHRF1 and reactivation of HIV-1 gene

253   expression and production from latency, a significant decrease in DNMT1 and in G9a/EHMT2 was

254   observed on the viral promoter (Fig. 3E, 3.61-fold decrease, p=0.0003 and 12.71-fold decrease,

255   p=0.00005, unpaired T test, for DNMT1 and G9a, respectively). These results thus indicate that UHRF1

256   silences HIV-1 gene expression during latency by actively promoting the accumulation of DNA

257   methylation on the viral promoter *via* its recruitment of DNMT1. Furthermore, we demonstrate that

258   UHRF1 also recruits G9a/EHMT2 to the latent promoter, thereby linking DNA methylation with the

259   accumulation of repressive histone methylation.

260   UHRF1 possesses multiple repression mechanisms of gene expression and our data suggest that

261   it can be recruited to the 5'LTR independently of DDMP5 methylation. We thus further dissected the

262   dependency of UHRF1 to DNA methylation and in particular, to the methylation status of DDMP5 for

263   its role in HIV-1 transcriptional repression. To do so, we subcloned the HIV-1 5'LTR region in a reporter

264   construct, where the LTR controls the firefly luciferase gene and is either unmethylated (referred as to

8

265   the "pLTR-FLuc" vector), in a hypermethylated state (i.e. where each CpG of the 5'LTR has been

266   artificially methylated, the resulting construct being termed "pLTRme-Fluc"), or where only the 5th CpG

267   dinucleotide corresponding to the DDMP5 of the LTR is methylated (referred as to the

268   "pLTR(CpG5me)-Fluc" vector). First, these three reporter vectors were transiently transfected in

269   HEK293T cells along with the control non-targeting shRNA vector (referred as to the "pshNT"). These

270   transfections showed that the pLTRme-Fluc vector presented a statistically significant decreased

271   luciferase activity in comparison to the pLTR-Fluc vector (Fig. 3F, 4.72-fold decrease, $p<0.0001$,

272   unpaired T test), confirming that methylation of the LTR provoked a decrease of its promoter activity.

273   Interestingly, methylation of the DDMP5 position alone was sufficient to reduce the LTR promoter

274   activity in a statistically relevant manner (Fig. 3F, 1.78-fold decrease, $p=0.0003$, unpaired T test), albeit

275   not as much as with the fully-methylated LTR (Fig. 3F, 2.64-fold increase, $p=0.0003$, unpaired T test).

276   These data confirmed the importance of DDMP5 methylation in recapitulating DNA methylation-

277   mediated repression on the HIV-1 promoter. Second, we transiently co-transfected the reporter LTR

278   constructs along with the UHRF1-targeting shRNA vector ("pshUHRF1"). Downregulation of

279   endogenous UHRF1 in HEK293T cells was confirmed by western blot (Fig. 3G) and was associated

280   with statistically significant increased luciferase activities for all three constructs (Fig. 3F, 10.77-fold

281   increase, $p<0.0001$; 1.83-fold increase, $p=0.0014$ and 4.71-fold increase, $p=0.0152$, for the pLTR-Fluc,

282   pLTRme-Fluc and pLTR(CpG5me)-Fluc constructs, respectively and according to an unpaired T test),

283   confirming the repressive role of UHRF1 in the control of HIV-1 gene expression. Interestingly, in this

284   reporter system, UHRF1-mediated repression of the HIV-1 promoter activity was proportionally lower

285   when the LTR was totally methylated or methylated on the DDMP5 in comparison to the repression

286   observed when the LTR was unmethylated (Fig. 3F, compare the 1.83-fold and 4.71-fold increases with

287   the 10.77-fold increase, for the fully-methylated, DDMP5-methylated and unmethylated LTRs,

288   respectively). These results indicated that UHRF1 repressive activity was dependent on the HIV-1

289   promoter DNA methylation status, and in particular, that this repression was partially, but not totally,

290   dependent on the DDMP5 methylation status. To confirm the dependency of UHRF1 on DNA

291   methylation for its role in HIV-1 transcriptional repression, we performed a rescue experiment in which

292   we transiently co-transfected reporter constructs along with the UHRF1-targeting shRNA vector then,

293   after twenty-four hours, we added an UHRF1 expression vector ("pUHRF1") before assaying the

294   luciferase activities after another twenty-four hours. Overexpression of UHRF1 was confirmed by

295   western blot (Fig. 3G) and decreased the luciferase activities of all three reporter vectors in comparison

296   to the conditions of UHRF1 downregulation (Fig. 3F, 3.88-fold decrease, $p<0.0001$; 1.80-fold decrease

297    $p=0.0217$ and 6.09-fold decrease, $p=0.0114$ for the pLTR-Fluc, pLTRme-Fluc and pLTR(CpG5me)-

298   Fluc constructs, respectively), thereby confirming the specific role of UHRF1 in the repression of HIV-

299   1 promoter activity. In particular, this effect was proportionally more important for the DDMP5-

300   methylated construct, then for the fully-methylated construct, in comparison to the unmethylated LTR

301   construct (Fig. 3F, compare the 6.09-fold and 1.80 -fold to the 3.89-fold, for the DDMP5-methylated,

9

302   fully-methylated and unmethylated LTRs, respectively). Together, these results indicated that in the

303   context of an *in vitro* HIV-1 5'LTR reporter system, UHRF1 repression of viral transcription depended

304   in part but not exclusively on DNA methylation of the viral promoter. Importantly, our system allowed

305   to specifically dissect the contribution of the single DDMP5 methylation status, showing its role in the

306   repression of HIV-1 promoter activity.

307   Altogether, our results demonstrated the DNA methylation-mediated role of UHRF1 in the HIV-

308   1 promoter silencing during latency.

Pharmacological downregulation of UHRF1 by EGCG promotes HIV-1 reactivation from latency.

310   Understanding the molecular mechanisms of HIV-1 latency has allowed the development of

311   several classes of LRAs (5). Our results on UHRF1 positioned this cellular factor as an attractive

312   pharmacological target for HIV-1 latency reversal strategies. Epigallocatechin-3-gallate (EGCG), the

313   major polyphenolic compound of green tea, has been shown to downregulate UHRF1 expression (37).

314   Accordingly, we showed that increasing concentrations of EGCG steadily decreased UHRF1 protein

315   levels starting from 30µg/mL of EGCG in J-Lat 8.4 cells (Fig. S5A). This protein level decrease was

316   not accompanied by a decrease in *UHRF1* mRNA level, as quantified by RT-qPCR (Fig. S5B),

317   consistent with a previous report showing that EGCG targets UHRF1 proteins but not *UHRF1*

318   transcripts (37).

319   To assess the LRA potential of EGCG *in vitro*, we quantified HIV-1 transcripts by RT-qPCR in

320   treated J-Lat 8.4 cells (Fig. 4A). We observed statistically significant increases in initiated (TAR region),

321   elongated (*gag* and *tat* regions), and MS HIV-1 transcript levels in EGCG-treated compared to mock-

322   treated conditions (Fig. 4A, 5.70-fold and p=0.03, 3.35-fold and p=0.003, 2.15-fold and p=0.003, and

323   3.11-fold increase and p=0.01 for TAR, *tat*, *gag* and MS RNA, respectively at 70µg/mL of EGCG).

324   Furthermore, quantification of GFP$^+$ cells by flow cytometry showed that starting from 10µg/mL of

325   EGCG, a release of the post-transcriptional blocks to the production of HIV-1 was observed (Fig. 4B).

326   In addition, the cellular metabolic activity in J-Lat 8.4 cells after treatment with increasing EGCG doses

327   was decreased in a statistically relevant manner, with a metabolic activity of 36% observed at the highest

328   EGCG dose (Fig. 4C). Despite increased levels of *gag* transcripts (Fig. 4A), EGCG did not reactivate

329   HIV-1 protein production in J-Lat 8.4 cells, as measured by p24^{Gag} capsid protein ELISA in cell

330   supernatants (Fig. S5C). These data were consistent with a previous report indicating that EGCG

331   destabilizes HIV-1 particles by binding to envelope phospholipids, thereby inducing their deformation

332   (38).

333   Since EGCG is a broad-acting compound (39), we next investigated EGCG modes of action in

334   HIV-1 latency reversal, specifically, their dependency on UHRF1 downregulation. First, we performed

335   EGCG reactivation assays in latently-infected J-Lat 8.4 cells in which UHRF1 expression had been

336   downregulated. By normalizing each EGCG treatment to its respective mock control, we observed a

337   statistically-significant decrease in EGCG reactivation potency in shUHRF1-transduced versus mock-

338   transduced cells (Fig. 4D, 6.34-fold decrease, p=0.0032, unpaired T test), whereas UHRF1 expression

10

was further downregulated in EGCG-treated shUHRF1-transduced cells in comparison to mock-treated, mock-transduced cells (Fig. 4E and Fig. 4F). Second, we assessed the DNA methylation signatures occurring at genome-scale while knocking down UHRF1 or treating latently-infected cells with EGCG and compared them. To do so, we performed an Infinium Human Methylation 850K array (40). By using unsupervised analyses, such as hierarchical clustering and principal component analyses, we revealed a strong effect of both EGCG treatment and UHRF1 knockdown on the cellular methylome, with treated samples being distinctly different from control samples (Fig. S6A and Fig. S6B). In addition, EGCG treatment and UHRF1 knockdown methylation profiles partially clustered together, suggesting that the effect of the two conditions on the DNA methylome is only partly similar. We identified 3664 hypomethylated CpGs through UHRF1 knockdown and 34614 hypomethylated CpGs through EGCG treatment (Fig. 4G and Fig. 4H, respectively). As already suggested by the unsupervised analyses, the overlap between differential CpGs through EGCG treatment and UHRF1 knockdown, while small, was statistically significant (Fig. 4I, 601 sites, hypergeometrical p-value < 1e-170), suggesting that some but not all mechanisms involved in the two processes were similar. We further assessed which pathways were affected at the DNA methylation level in EGCG-treated and shUHRF1-transduced conditions using a Gene Set Enrichment Analysis (GSEA)(41). This analysis further confirmed the partial but not total overlap between the two conditions (Fig. S6C and S6D).

Together, these experiments indicated that EGCG reactivates HIV-1 from latency in part *via* the downregulation of UHRF1, although, this compound has a broader reactivation capacity on HIV-1 gene expression, in line with its pleiotropic action on the HIV-1 replication cycle (38, 42).

EGCG induces HIV-1 expression in CD8$^+$-depleted PBMCS from HIV-1$^+$ aviremic individuals.

The development of LRAs has been guided by deciphering HIV-1 latency molecular mechanisms in *in vitro* cell models (5). However, these models do not completely recapitulate the biological properties of *in vivo* latent reservoirs (43). Therefore, we next evaluated the LRA potency of EGCG *ex vivo*, using cultures of CD8$^+$-depleted PBMCs isolated from blood of cART-treated aviremic HIV-1$^+$ individuals.

We first assessed cellular viability and metabolic activity in *ex vivo* cultures of CD8$^+$-depleted PBMCs from six healthy donors in response to EGCG treatments (Fig. S7). Neither TCR stimulation, serving as a positive control, nor increasing EGCG doses affected cellular viability (Fig. S7A). However, consistent with our observations in J-Lat cells, metabolic activity was affected by EGCG, although the median of metabolic activity remained tolerable (Fig. S7B). Suitable LRA candidates for anti-HIV-1 latency strategies *in vivo* should limit non-specific or strong immune T-cell activation. Therefore, we assessed the level of cell surface activation markers HLA-DR (late activation marker), CD25 (intermediate activation marker), CD69 (early activation marker) and CD38 (late activation marker and predictor of HIV-1 progression) in comparison to the mock-treated condition (Fig. S7C-F). TCR stimulation consistently and statistically increased the levels of each marker, while EGCG treatment increased slightly but statistically the surface expression of CD69 (Fig. S7E). Because this increase in

11

376   CD69 expression was not associated with later cell activation when EGCG stimulation was sustained

377   for 6 days (data not shown), we attributed it to an indirect epigenetic effect of EGCG (44). Flow

378   cytometry analyses also highlighted that increasing doses of EGCG were associated with a statistically

379   significant decrease in CD4 expression on the treated CD8$^+$-depleted PBMCs (Fig. S7G), which would,

380   in the context of HIV-1 infection, reduce the number of target cells and therefore limit HIV-1

381   dissemination.

382   Based on these observations of tolerable cytotoxic, metabolic and immune effects, we next

383   investigated HIV-1 recovery in CD8$^+$-depleted PBMCs in response to EGCG treatments. To do so, we

384   purified CD8$^+$-depleted PBMCs from 22 HIV$^+$ aviremic cART-treated individuals (Table S1A) and

385   evaluated the frequency of infected cells during plating by quantification of cell-associated total HIV-1

386   DNA (Table S1B). *Ex vivo* cultures were then mock-treated, treated with 50µg/mL or 70µg/mL of

387   EGCG or activated with anti-CD3 + anti-CD28 antibodies as a positive control. Because of EGCG effect

388   in degrading viral particles, reactivation of HIV-1 gene expression was measured unequivocally by the

389   quantification of intracellular HIV-1 RNA. These quantifications showed that EGCG potently increased

390   HIV-1 unspliced RNA levels in patient cells, even to higher levels than TCR activation (Fig. 5A).

391   Moreover, HIV-1 US RNA/DNA ratios were statistically increased in EGCG-treated conditions (Fig.

392   S8A and S8C), indicating that proviruses were more transcriptionally active. Quantification of HIV-1

393   extracellular RNA in supernatants, serving as a surrogate for the completion of the viral replication

394   cycle, further indicated a statistically significant increase in HIV-1 extracellular RNA when CD8$^+$-

395   depleted PBMCs from HIV$^+$ individuals were submitted to EGCG treatments (Fig. 5B). Thus our result

396   show that, by destabilizing HIV-1 particles in reactivated cell cultures (38), EGCG treatment released

397   HIV-1 RNA from virions *ex vivo*. Accordingly, we observed a statistically-significant increase in HIV-

398   1 extracellular RNA/DNA ratios in EGCG-treated compared to mock-treated *ex vivo* patient cell cultures

399   (Fig. S8B and S8C), indicating that not only transcriptional but also post-transcriptional latency blocks

400   were overcome by EGCG treatment. Altogether, our results highlight the strong potency of EGCG as a

401   new LRA *ex vivo* allowing to reactivate HIV-1 transcription to the completion of the replication cycle,

402   while maintaining low immune activation level, and even allowing to prevent *de novo* infections by

403   decreasing cell surface CD4 marker expression and by degrading reactivated HIV-1 particles.

404   Finally, because our *in vitro* data pointed to the pleiotropic action of EGCG in its HIV-1

405   reactivation capacity, we further assessed the contribution of HIV-1 promoter methylation *ex vivo* to

406   EGCG reactivation potency. A dynamical increase in the degree of viral promoter methylation has been

407   shown in HIV$^+$ individuals in response to the duration of the antiretroviral treatment or the time of viral

408   suppression (16, 17). Accordingly, strong statistically significant positive correlations were observed

409   between the EGCG-mediated HIV-1 reactivation potency and either time on cART (Fig. S9A) or time

410   of virological suppression (Fig. S9B), while no correlation was observed for the positive control (Fig.

411   S9C). These results demonstrate that EGCG modes of action *ex vivo* are time-dependent in HIV$^+$

412   individuals, suggesting that EGCG acts, at least in part, through HIV-1 promoter demethylation. To

12

413   refine this observation, we next assessed the DNA methylation level of the viral promoter in our cohort

414   of HIV[+] individuals by sodium bisulfite sequencing. As suggested by Blazkova and colleagues (10), we

415   found that the assessment of DNA methylation in aviremic individuals, who have smaller reservoirs that

416   prevent the analysis of proviral DNA, was technically challenging. Nevertheless, we obtained the DNA

417   methylation profile of the HIV-1 promoter for 8 out of the 22 enrolled HIV+ individuals. Out of these,

418   five individuals had no detectable DNA methylation, while three individuals presented a median

419   methylation level of 7.41% mCpG on the HIV-1 promoter, which corresponds to levels reported in other

420   studies (10, 12, 17). To determine the relationship between EGCG reactivation potency and *in vivo* HIV-

421   1 promoter methylation, we clustered these 8 individuals in groups of non-methylated or methylated

422   5'LTR and plotted the cell-associated HIV-1 US RNA for 50μg/mL of EGCG (Figure S9D). Without

423   reaching statistical significance, a trend towards a higher reactivation could be observed for patients

424   accumulating more DNA methylation on the viral promoter. The lack of statistical significance can be

425   attributed to the low number of patients but it also reveals the pleiotropic reactivation capacity of EGCG.

426   We propose that the mechanism of EGCG reactivation of HIV-1 from latency is through DNA

427   demethylation of the viral promoter, or, when it is not methylated, through indirect demethylation of

428   cellular genes.

429   Altogether, our *ex vivo* data indicate, in line with the heterogeneity of the mechanisms responsible

430   for HIV-1 latency, that EGCG, in addition to its antiviral properties, is a heterogeneous LRA, capable

431   of reversing HIV-1 latency through several modes of actions depending on different infected

432   individuals.

433

434   **DISCUSSION**

435   Accumulating data highlights the intrinsically dynamic and heterogeneous nature of latent HIV-

436   1 cellular reservoirs within and between infected individuals. This heterogeneity and the multiplicity of

437   the silencing mechanisms underlying HIV-1 latency rather than latency in itself are now considered as

438   the major barrier to eradicating HIV-1 (8). In agreement, LRAs have been found to present various

439   reactivation potencies *in vitro* and *ex vivo* (45–47). In the context of DNA methylation, our previous

440   study has highlighted that the DNA methylation inhibitor 5-AzadC exhibits different *ex vivo* reactivation

441   potencies in terms of HIV-1 latency reversal (18). Here, we investigated the molecular source of this

442   potency heterogeneity at the level of proviral DNA methylation.

443   We first evidenced the existence of non-random and reproducible DNA methylation signatures in

444   response to 5-AzadC treatment at the level of the single CpG dinucleotide in the HIV-1 promoter. Thus,

445   rather than reactivating HIV-1 in a non-specific manner, 5-AzadC acts through specific molecular

446   mechanisms within the viral promoter. To tease out for these regulatory mechanisms, we mapped

447   preferentially-demethylated positions in the 5'LTR. In the present study, we focused on the most

448   significantly-demethylated CpG position of our whole dataset but a similar approach can be used for

449   other positions or for other epigenetic LRAs. DDMP5 is located in a CRE, however, rather than showing

13

450   that DDMP5 methylation prevents the binding of cognate transcriptional activators (22, 48), we

451   demonstrated that DDMP5 methylation allowed the *in vitro* binding of an additional protein complex,

452   containing UHRF1. We also reported *in vivo* recruitment of UHRF1 to the latent HIV-1 promoter.

453   Interestingly, we showed that UHRF1 recruitment to the latent promoter was only proportional to the

454   level of DDMP5 methylation, indicating that UHRF1 could be recruited redundantly to the latent

455   promoter through other mechanisms than DNA methylation. This redundancy is a general trend in the

456   recruitment of epigenetic machineries to the HIV-1 5'LTR and safeguarding their recruitment points

457   towards the importance of the epigenetic repression of viral genes during latency (8). UHRF1, in

458   particular, is an important epigenetic integrator as it both reads the chromatin (5mC, H3K9me3 and

459   H3R2) and recruits epigenetic enzymes (DNMT1, G9a/EHMT2, …). We thus investigated the role of

460   the recruited UHRF1 in participating in the 5'LTR heterochromatinization during HIV-1 latency. We

461   report here for the first time a role for UHRF1 in HIV-1 silencing through DNA methylation.

462   Mechanistically, UHRF1 knockdown led to a statistically significant decrease in the global DNA

463   methylation level of the 5'LTR and of DNMT1 recruitment. We also showed that G9a/EHMT2

464   recruitment to the 5'LTR was decreased upon UHRF1 knockdown, supporting the model that UHRF1

465   branches several repressive epigenetic mechanisms during HIV-1 latency. Considering the multiple

466   modes of gene repression mediated by UHRF1, we further sought to determine how much of its

467   repressive action on the 5'LTR was dependent on DNA methylation, and in particular on the methylation

468   status of DDMP5. To answer unambiguously to this question, we decided to work in an artificial system

469   of transient transfection and showed that, even there, UHRF1 repression of HIV-1 transcription

470   depended strongly on DNA methylation and, in a large part, on DDMP5. Thus, in agreement with its

471   potential multiple recruitment modes to the viral promoter, UHRF1 represses HIV-1 gene expression

472   during latency through several mechanisms, but predominantly, through DNA methylation. Together,

473   these results demonstrate that UHRF1 is a new actor in HIV-1 latency.

474   As a proof-of-concept that the molecular characterization of HIV-1 latency leads to the

475   identification of new targets for therapeutic strategies, we next studied the latency-reversing potency of

476   UHRF1 downregulation. EGCG, the major phenolic compound of green tea, has been reported, among

477   other functions, to affect UHRF1 expression (49). Using complementary models – latently-infected J-

478   Lat T-cell lines and *ex vivo* cell cultures from cART-treated HIV⁺ aviremic individuals – our results

479   showed the potency of EGCG as a new LRA. Indeed, EGCG reactivated HIV-1 from latency up to the

480   completion of the viral replication cycle, in a short time frame, and in all the latency models we tested.

481   Interestingly, EGCG had been reported to present an antiviral activity on HIV-1, by inhibiting several

482   steps of its replication cycle, notably, by binding and destabilizing the HIV-1 envelope (38). This has

483   led to its use in anti-HIV clinical trials (NCT01433289 and NCT03141918, ClinicalTrials.gov). In

484   agreement with EGCG antiviral activity on HIV-1 (38), we detected little p24^{Gag} capsid protein in the

485   cell culture supernatants in our reactivation experiments. We nevertheless observed, in our *ex vivo*

486   patient cell cultures, that EGCG augmented the recovery of extracellular HIV-1 RNA. Thus, these

487   results suggest that reactivated virions were indeed destabilized by EGCG in cell culture supernatants.

488   Furthermore, we showed that EGCG treatment was associated with a decreased expression of the

489   cellular surface marker CD4 on target cells, thereby preventing subsequent new infections following

490   reactivation. We thus showed the promising use of EGCG in HIV-1 eradication strategies due to its

491   complementary and synergistic anti-HIV modes of action. On a larger perspective, we also showed the

492   relevance of targeting UHRF1 in HIV-1 cure therapeutic strategies, in trend with the considerable

493   attention for UHRF1 inhibitors in the cancer field (49). Our results indicate, however, that EGCG

494   potency is not uniquely dependent on UHRF1 expression, rather this compound presents a pleiotropic

495   function in HIV-1 reactivation, balancing the heterogeneity observed in viral reservoirs.

496   In conclusion, we developed a probabilistic methodology to decipher the DNA methylation-

497   mediated mechanisms underlying the heterogeneous capacity of 5-AzadC to reactivate HIV-1 from

498   latency. This approach enabled us to uncover the role of UHRF1, an epigenetic integrator, in HIV-1

499   promoter silencing *via* DNA methylation. Our work provides a demonstration that the understanding of

500   the molecular basis of the heterogeneous effects of LRAs, even in *in vitro* HIV-1 latency models, can

501   bring to light new factors involved in HIV-1 silencing and hence, new targets to devise anti-HIV

502   therapeutic approaches. As a proof-of-concept, we showed that EGCG, a known inhibitor of UHRF1,

503   presents, in addition to its broad antiviral activities, a pleiotropic anti-latency activity, allowing its

504   potential use in HIV-1 cure strategies.

ACKNOWLEDGMENTS

AUTHOR CONTRIBUTIONS

Conceived and designed the experiments: CVL, RV and SB. Performed the experiments: RV, SB, LN, GD, CV, AA-A, MB, EP, ND. Performed the HIV-1 DNA and RNA quantifications: AP, GD, VAF and AC. Performed the activation analyses: FC. Performed the primary models of HIV latency experiments: VLD, VG. Performed the Infinium analyses: MB and FF. Performed the ultra-sensitive p24 assays: AS-C. Performed HIV[+] individuals selection: CN, SDW. Analyzed the data: RV, SB, LN, GD, CV, AA-A, MB, EP, ND and CVL. Contributed in reagents/materials/analysis tools: CS, CR, BB, VG, OR. Wrote the paper: RV, SB and CVL.

16

540 **MATERIAL AND METHODS**

541 **Cell culture**

542 Jurkat, J-Lat 6.3, J-Lat 8.4, J-Lat 9.2, J-Lat 15.4 and the HEK293T cell lines were obtained from

543 the AIDS Research and Reference Reagent Program (NIAID, NIH). Cells were grown in RPMI 1640

544 medium (Gibco-BRL) supplemented with 10 % fetal bovine serum, 50 U/ml of penicillin and 50 µg/mL

545 of streptomycin and were cultivated at 37°C in a 5% CO_2 atmosphere.

546 **Reagents and antibodies**

547 5-aza-2'-deoxycytidine (5-AzadC, A3656) and epigallocatechin-3-gallate (EGCG, E4143) were

548 purchased from Sigma Aldrich. Antibodies against CREB (sc-186), CREM (sc-440), ATF-1 (sc-28673),

549 MBD4 (sc-10753) and purified rabbit IgG (sc-2027) were purchased from Santa Cruz Biochemical.

550 Antibodies against MBD1 (pAb-078-050) and UHRF1 (H00029128-B01P) were purchased from

551 Diagenode and Abnova, respectively. Antibodies against MBD2/3 (07-199) and Kaiso (05-659) were

552 purchased from Upstate/Millipore. Antibodies against MeCP2 (ab2828) and RBP-JK (ab33065) were

553 purchased from Abcam. Antibodies against RNAPII (14958) were purchased from Cell Signaling.

554 Secondary antibodies were purchased from Cell Signaling (7074 and 7076).

555 **Virus production assays**

556 HIV-1 production was measured in cell culture supernatants of cell cultures by ELISA assays on

557 p24^{Gag} using the INNOTEST HIV Antigen mAb kit per the manufacturer's instructions (Fujirebio).

558 **Sodium Bisulfite-mediated mapping of methylcytosines**

559 Genomic DNA was isolated using the DNeasy Blood and Tissue kit (Qiagen), then sodium

560 bisulfite-converted (EpiTect Bisulfite kit, Qiagen). The 5'LTR or the *rev* regions were amplified by

561 (semi)nested PCR (primer sequences are available upon request). At least 12 clones from each condition

562 were sequenced, and clones with sodium bisulfite conversion higher than 95% were aligned on the HIV-

563 1 NL4.3 reference sequence using ClustalΩ. MethTools (50) and Inkscape were used for graphical

564 representations.

565 **Electrophoretic Mobility Shift Assays (EMSAs)**

566 Nuclear extracts were prepared using a protocol described by Dignam and colleagues (51).

567 EMSAs, competition EMSAs and supershift assays were performed as described previously (48).

568 **Chromatin Immunoprecipitation assays**

569 ChIP assays were performed as previously described (52), using the ChIP assay kit from Millipore

570 or equivalent homemade solutions. Relative quantification using standard curve method on the input

571 was performed for each primer pair and 96-well Optical Reaction plates were read in a StepOnePlus

572 PCR instrument (Applied Biosystems). Fold enrichments were calculated as fold inductions relative to

573 the values measured with IgG. Primer sequences used for quantification are available upon request.

574 **Western Blot**

575 Western blotting was performed with 15µg of total protein extracts. The immunodetection was

576 assessed using primary antibodies targeting UHRF1 or β-actin as loading control. Horseradish

577   peroxidase (HRP)-conjugated secondary antibodies were used for chemiluminescence detection (Cell

578   Signaling).

579   **RNA extraction and analysis of transcripts**

580   Total RNA samples were isolated using the Tri-Reagent (TRC-118, MRC), according to the

581   manufacturer's protocol. Following DNAse treatment (AM1907, Invitrogen), reverse transcription was

582   performed with the PrimeScript RT reagent kit (RR037A, TaKaRa).

583   **Lentiviral production and transduction assays**

584   TRC Lentiviral shRNA plasmids (pLKO.1) MISSION shRNA were obtained from Sigma-

585   Aldrich (SHC002, TRCN0000273315, TRCN0000273256, TRCN0000273317 and TRC0000004352).

586   The pMD2.G and the psPAX2 packaging system were obtained from Addgene. VSV-G pseudotyped

587   particles were produced by transfection of HEK 293T cells as described previously(33). J-Lat cells were

588   transduced as described previously (53).

589   **Cellular proliferation assays and viability**

590   Cellular proliferation was evaluated by the colorimetric test WST-1 according to the

591   manufacturer's instructions (Roche). Cellular viability was assessed by staining the cells with the

592   LIVE/DEAD Fixable Near-IR Dead Cell Stain (Thermo Fisher) and analysis by flow cytometry on a

593   FACSCantoII (Becton-Dickinson), using the FACSDiva Software (Becton-Dickinson).

594   **Plasmid constructs and reporter assays**

595   The human UHRF1 expression vector (pCMV-HA-UHRF1, termed pUHRF1) was kindly

596   provided by Dr Olivier Rohr. The non-episomal pLTR-Fluc vector was described previously (54). To

597   obtain the pLTRme-Fluc vector, where only the LTR CpGs are methylated, we methylated *in vitro* the

598   whole pLTR-Fluc construct using the SssI methyltransferase (New England Biolabs, M0226). The LTR

599   fragment was then purified, cloned back in the parental reporter vector and the resulting pLTRme-Fluc

600   vector was directly transfected without bacterial amplification.

601   **Infinium 850K Human Methylation arrays**

602   Genomic DNA was extracted with the DNeasy Blood and Tissue Kit (QIAGEN) and converted

603   with sodium bisulfite (EZ DNA Methylation Kit, Zymo Research). The quality of each analyzed sample

604   was first evaluated by inspection of the control probes intensity level. Raw data (uncorrected probe

605   intensity values) from the Infinium Methylation arrays were processed according to the recommended

606   steps of Dedeurwaerder *et al.*(55). Beta-values were computed using the following formula: Beta-value

607   = M/[U+M] where M and U are the raw "methylated" and "unmethylated" signals, respectively. Beta-

608   values were corrected for type I and type II bias using the peak-based correction (56). Infinium

609   HumanMethylation850K raw data were submitted to the NCBI's Gene Expression Omnibus (GEO)

610   database (GSE139320, token : wnqfssiudxubtgx). Principal component analysis and hierarchical

611   clustering were performed via an in-house R script using the most variable Infinium probes (standard

612   deviation ≥ 0.27). For differential analysis, probes showing an absolute difference between case and

613   control Beta-values higher than 0.3 were assumed significant. For pathway analysis, Infinium probes

18

614 located in promoter regions were first associated to their corresponding genes. Then, a « delta-Beta »

615 was defined for each gene as the difference between case and control Beta-values of its promoter

616 Infinium probe showing the highest absolute difference. Finally, genes were ranked according to their

617 delta-Beta and submitted to the GSEA tool (41) to search for significant enrichments among the

618 HALLMARK gene sets from MSigDB (http://software.broadinstitute.org/gsea/msigdb/).

619 **Study subjects**

620 We selected 22 HIV-1-infected individuals at the Saint-Pierre Hospital (Brussels, Belgium) based

621 on the following criteria: all volunteers were treated with cART for at least 1 year, had an undetectable

622 plasma HIV-1 RNA level (20 copies/ml) for at least 1 year, and had a level of CD4+ T lymphocytes

623 higher than 300 cells/mm^3 of blood. Characteristics (age, CD4+ T cell count, CD4+ nadir, antiviral

624 regimens, duration of therapy, duration with undetectable plasma HIV-1 RNA level, and HIV-1

625 subtypes) of HIV$^+$ individuals from the Saint-Pierre Hospital were well documented and are presented

626 in Table S1A. Buffy coats from healthy donors were obtained at the Belgian Red Cross.

627 **Ethical statement**

628 Ethical approval was granted by the Human Subject Ethics Committee of the Saint-Pierre Hospital

629 (Brussels, Belgium). All individuals enrolled in the study provided written informed consent for

630 donating blood.

631 **Isolation of CD8$^+$-depleted PBMCs**

632 CD8$^+$-depleted PBMCs used in reactivation assays were isolated from fresh whole blood of HIV$^+$

633 individuals as previously described (18).

634 **Quantitation of cell-associated HIV-1 unspliced RNA**

635 Total nucleic acids were extracted from pellets of CD8$^+$-depleted PBMCs according to the Boom

636 isolation method (57). Extracted cellular RNA was treated with DNase (DNA-free kit; Thermo Fisher

637 Scientific) and reverse transcribed using the SuperScript III reverse transcriptase (Thermo Fisher

638 Scientific). cDNA was used for the qPCR-based quantification of cell-associated HIV-1 unspliced RNA

639 (amplicon in the *gag* region), as previously reported (58). HIV-1 RNA copy numbers were normalized

640 to the total cellular RNA (by measurement of 18S ribosomal RNA) inputs as described previously (59).

641 Non-template control wells were included in every qPCR run and were consistently negative.

642 **Quantification of HIV-1 extracellular RNA**

643 Total RNA was extracted from CD8$^+$-depleted PBMCs *ex vivo* culture supernatants using the QIA

644 amp Viral RNA Mini kit (Qiagen). HIV-1 RNA levels were quantified using the Generic HIV Viral

645 Charge kit (Biocentric) according to the manufacturer's instructions.

646 **Quantification of total HIV-1 DNA**

647 Total cellular DNA was extracted from patient CD8$^+$-depleted PBMCs *ex vivo* cultures using the

648 QIAamp DNA Mini kit (Qiagen). The total cell-associated HIV-1 DNA was then quantified by ultra-

649 sensitive real-time PCR (Generic HIV DNA cell kit, Biocentric) according to the manufacturer's

650 instruction (60).

19

651 **Cell activation analysis by flow cytometry**

652   For cell activation analysis, CD8$^+$-depleted PBMCs from blood of healthy donors were used to

653 establish *ex vivo* cell cultures. Cells were collected 24 hours after stimulation with EGCG and were

654 stained with relevant antibodies as previously described (18).

655 **Statistical analysis**

656   The demethylation probability following 5-AzadC treatment was calculated as follows:

657

$$P(\text{demeth}) = 1 - \left(1 - \frac{\#D(\text{treated})}{\#C(\text{total})}\right) \times \frac{\#C(\text{total})}{\#M(\text{mock})}$$

658 where P(demeth) corresponds to the probability of demethylation following treatment, #D(treated) the

659 number of demethylated CpGs in the treated conditions, #C(total) the number of clones (12 for each

660 condition in the present study) and where #M(mock) corresponds to the number of methylated CpGs in

661 the mock-treated conditions. Sodium bisulfite sequencing data sets were analyzed using Fisher's exact

662 test. For all the analyses, the threshold of statistical significance was set at 0.05. p-values $\leq$ 0.05 (*: p-

663 value $\leq$ 0.05, **: p-value $\leq$ 0.01, ***: p-value $\leq$ 0.001) were considered statistically significant. All tests

664 were two-sided. All analyses were performed using Prism version 6.0 (GraphPad software) and

665 Microsoft Excel. Statistical tests are indicated in the corresponding figure legends.

666

REFERENCES

1. Deeks S, Autran B, Berkhout B, Benkirane M, Cairns S, Chomont N, Chun T-W, Churchill M, Di Mascio M, Katlama C, Lafeuillade A, Landay A, Lederman M, Lewin S, Maldarelli F, Margolis D, Markowitz M, Martinez-Picado J, Mullins J, Mellors J, Moreno S, O'Doherty U, Palmer S, Penicaud M-C, Peterlin M, Poli G, Routy J-P, Rouzioux C, Silvestri G, Stevenson M, Telenti A, Van Lint C, Verdin E, Woolfrey A, Zaia J, Barré-Sinoussi F. 2012. Towards an HIV cure: a global scientific strategy. Nat Rev Immunol 12:607–14.

2. Trono D, Van Lint C, Rouzioux C, Verdin E, Barré-Sinoussi F, Chun T-W, Chomont N. 2010. HIV persistence and the prospect of long-term drug-free remissions for hiv-infected individuals. Science (80-) 329:174–180.

3. Chun T-WW, Fauci AS. 2012. HIV reservoirs: Pathogenesis and obstacles to viral eradication and cure. AIDS 26:1261–1268.

4. Darcis G, Van Driessche B, Van Lint C. 2017. HIV Latency: Should We Shock or Lock? Trends Immunol 38:217–228.

5. Spivak A, Planelles V. 2018. Novel Latency Reversal Agents for HIV-1 Cure. Annu Rev Med 69:421–436.

6. Mbonye U, Karn J. 2017. The Molecular Basis for Human Immunodeficiency Virus Latency. Annu Rev Virol 4:261–285.

7. Lange UC, Verdikt R, Ait-Ammar A, Van Lint C. 2020. Epigenetic crosstalk in chronic infection with HIV-1. Semin Immunopathol 42:187–200.

8. Verdikt R, Hernalsteens O, Lint C Van. 2021. Epigenetic Mechanisms of HIV-1 Persistence. Vaccines 9:1–23.

9. Kauder S, Bosque A, Lindqvist A, Planelles V, Verdin E. 2009. Epigenetic regulation of HIV-1 latency by cytosine methylation. PLoS Pathog 5:1–15.

10. Blazkova J, Trejbalova K, Gondois-Rey F, Halfon P, Philibert P, Guiguen A, Verdin E, Olive D, Van Lint C, Hejnar J, Hirsch I. 2009. CpG methylation controls reactivation of HIV from latency. PLoS Pathog 5:1–14.

11. Chavez L, Kauder S, Verdin E. 2011. In vivo, in vitro, and in silico analysis of methylation of the HIV-1 provirus. Methods 53:47–53.

12. Palacios JA, Pérez-Piñar T, Toro C, Sanz-Minguela B, Moreno V, Valencia E, Gómez-Hernando C, Rodés B. 2012. Long-term nonprogressor and elite controller patients who control viremia have a higher percentage of methylation in their HIV-1 proviral promoters than aviremic patients receiving highly active antiretroviral therapy. J Virol 86:13081–4.

13. Blazkova J, Murray D, Justement JS, Funk E, Nelson A, Moir S, Chun T-W, Fauci A. 2012. Paucity of HIV DNA Methylation in Latently Infected, Resting CD4+ T Cells from Infected Individuals Receiving Antiretroviral Therapy. J Virol 1–10.

14. Ho Y-C, Shan L, Hosmane N, Wang J, Laskey S, Rosenbloom D, Lai J, Blankson J, Siliciano J, Siliciano R. 2013. Replication-competent noninduced proviruses in the latent reservoir increase barrier to HIV-1 cure. Cell 155:540–51.

15. Weber S, Weiser B, Kemal KS, Burger H, Ramirez CM, Korn K, Anastos K, Kaul R, Kovacs C, Doerfler

W. 2014. Epigenetic analysis of HIV-1 proviral genomes from infected individuals: Predominance of unmethylated CpG's. Virology 449:181–9.

16. Trejbalova K, Kovarova D, Blazkova J, Machala L, Jilich D, Weber J, Kucerova D, Vencálek O, Hirsch I, Hejnar J. 2016. Development of 5' LTR DNA methylation of latent HIV-1 provirus in cell line models and in long-term-infected individuals. Clin Epigenetics 8:1–20.

17. Cortés-Rubio CN, Salgado-Montes de Oca G, Prado-Galbarro FJ, Matías-Florentino M, Murakami-Ogasawara A, Kuri-Cervantes L, Carranco-Arenas AP, Ormsby CE, Cortés-Rubio IK, Reyes-Terán G, Ávila-Ríos S. 2019. Longitudinal variation in human immunodeficiency virus long terminal repeat methylation in individuals on suppressive antiretroviral therapy. Clin Epigenetics 11:1–17.

18. Bouchat S, Delacourt N, Kula A, Darcis G, Van Driessche B, Corazza F, Gatot J-S, Melard A, Vanhulle C, Kabeya K, Pardons M, Avettand-Fenoel V, Clumeck N, Wit S De, Rohr O, Rouzioux C, Van Lint C. 2015. Sequential treatment with 5-aza-2'-deoxycytidine and deacetylase inhibitors reactivates HIV- 1. EMBO Mol Med 8:1–22.

19. Pereira L, Bentley K, Peeters A, Churchill M, Deacon N. 2000. A compilation of cellular transcription factor interactions with the HIV-1 LTR promoter. Nucleic Acids Res 28:663–8.

20. Jones C, Kadonaga JT, Luciw P, Tjian R. 1986. Activation of the AIDS Retrovirus Promoter by the Cellular Transcription Factor, Sp1. Science (80-) 232:755–759.

21. Van Lint C, Amella CA, Emiliani SS, John M, Jie T, Verdin E. 1997. Transcription Factor Binding Sites Downstream of the Human Immunodeficiency Virus Type 1 Transcription Start Site Are Important for Virus Infectivity. J Virol 71:6113–6127.

22. Zhang X, Odom DT, Koo S-HH, Conkright MD, Canettieri G, Best J, Chen H, Jenner R, Herbolsheimer E, Jacobsen E, Kadam S, Ecker JR, Emerson B, Hogenesch JB, Unterman T, Young RA, Montminy M. 2005. Genome-wide analysis of cAMP-response element binding protein occupancy, phosphorylation, and target gene activation in human tissues. Proc Natl Acad Sci 102:4459–4464.

23. Bartels S, Spruijt C, Brinkman A, Jansen P, Vermeulen M, Stunnenberg H. 2011. A SILAC-Based Screen for Methyl-CpG Binding Proteins Identifies RBP-J as a DNA Methylation and Sequence- Specific Binding Protein. PLoS One 6:1–10.

24. Defossez P-A, Stancheva I. 2011. Biological functions of methyl-CpG-binding proteins., p. 377–98. *In* Progress in Molecular Biology and Translational Science.

25. Hashimoto H, Horton JR, Zhang X, Cheng X. 2009. UHRF1, a modular multi-domain protein, regulates replication-coupled crosstalk between DNA methylation and histone modifications. Epigenetics 4:8–14.

26. Fang J, Cheng J, Wang J, Zhang Q, Liu M, Gong R, Wang P, Zhang X, Feng Y, Lan W, Gong Z, Tang C, Wong J, Yang H, Cao C, Xu Y. 2016. Hemi-methylated DNA opens a closed conformation of UHRF1 to facilitate its histone recognition. Nat Commun 7:1–12.

27. Kim JK, Estève P-O, Jacobsen SE, Pradhan S. 2009. UHRF1 binds G9a and participates in p21 transcriptional regulation in mammalian cells. Nucleic Acids Res 37:493–505.

28. Unoki M, Nishidate T, Nakamura Y. 2004. ICBP90, an E2F-1 target, recruits HDAC1 and binds to methyl-CpG through its SRA domain. Oncogene 23:7601–10.

29. Hopfner R, Mousli M, Jeltsch JM, Voulgaris A, Lutz Y, Marin C, Bellocq JP, Oudet P, Bronner C. 2000. ICBP90, a novel human CCAAT binding protein, involved in the regulation of topoisomerase IIα

747   expression. Cancer Res 60:121–128.

748   30.   Sharif J, Muto M, Takebayashi S, Suetake I, Iwamatsu A, Endo T a, Shinga J, Mizutani-Koseki Y, Toyoda

749   T, Okamura K, Tajima S, Mitsuya K, Okano M, Koseki H. 2007. The SRA protein Np95 mediates

750   epigenetic inheritance by recruiting Dnmt1 to methylated DNA. Nature 450:908–12.

751   31.   Ashraf W, Ibrahim A, Alhosin M, Zaayter L, Ouararhni K, Papin C, Ahmad T, Hamiche A, Mély Y,

752   Bronner C, Mousli M. 2017. The epigenetic integrator UHRF1: on the road to become a universal

753   biomarker for cancer. Oncotarget 8:51946–51962.

754   32.   Pasternak AO, Adema KW, Bakker M, Jurriaans S, Berkhout B, Cornelissen M, Lukashov V V. 2008.

755   Highly sensitive methods based on seminested real-time reverse transcription-PCR for quantitation of

756   human immunodeficiency virus type 1 unspliced and multiply spliced RNA and proviral DNA. J Clin

757   Microbiol 46:2206–2211.

758   33.   Lusic M, Marini B, Ali H, Lucic B, Luzzati R, Giacca M. 2013. Proximity to PML nuclear bodies regulates

759   HIV-1 latency in CD4+ T cells. Cell Host Microbe 13:665–677.

760   34.   Bianchi C, Zangi R. 2013. UHRF1 discriminates against binding to fully-methylated CpG-Sites by steric

761   repulsion. Biophys Chem 171:38–45.

762   35.   Bashtrykov P, Jankevicius G, Jurkowska R, Ragozin S, Jeltsch A. 2013. The Uhrf1 protein stimulates the

763   activity and specificity of the maintenance DNA methyltransferase Dnmt1 by an allosteric mechanism. J

764   Biol Chem 0–18.

765   36.   Bostick M, Kim JK, Estève P-O, Clark A, Pradhan S, Jacobsen SE. 2007. UHRF1 plays a role in

766   maintaining DNA methylation in mammalian cells. Science (80-) 317:1760–4.

767   37.   Achour M, Mousli M, Alhosin M, Ibrahim A, Peluso J, Muller CD, Schini-Kerth V, Hamiche A, Dhe-

768   Paganon S, Bronner C. 2013. Epigallocatechin-3-gallate up-regulates tumor suppressor gene expression

769   via a reactive oxygen species-dependent down-regulation of UHRF1. Biochem Biophys Res Commun

770   430:208–12.

771   38.   Yamaguchi K, Honda M, Ikigai H, Hara Y, Shimamura T. 2002. Inhibitory effects of (−)-epigallocatechin

772   gallate on the life cycle of human immunodeficiency virus type 1 (HIV-1). Antiviral Res 53:19–34.

773   39.   Singh BN, Shankar S, Srivastava RK. 2011. Green tea catechin , epigallocatechin-3-gallate (EGCG):

774   Mechanisms, perspectives and clinical applications. Biochem Pharmacol 82:1807–1821.

775   40.   Moran S, Arribas C, Esteller M. 2016. Validation of a DNA methylation microarray for 850,000 CpG sites

776   of the human genome enriched in enhancer sequences. Epigenomics 8:389–399.

777   41.   Subramanian A, Tamayo P, Mootha VK, Mukherjee S, Ebert BL, Gillette MA, Paulovich A, Pomeroy SL,

778   Golub TR, Lander ES, Mesirov JP. 2005. Gene set enrichment analysis: A knowledge-based approach for

779   interpreting genome-wide expression profiles. Proc Natl Acad Sci U S A 102:15545–15550.

780   42.   Williamson MP, McCormick TG, Nance CL, Shearer WT. 2006. Epigallocatechin gallate, the main

781   polyphenol in green tea, binds to the T-cell receptor, CD4: Potential for HIV-1 therapy. J Allergy Clin

782   Immunol 118:1369–1374.

783   43.   Spina CA, Anderson J, Archin NM, Bosque A, Chan J, Famiglietti M, Greene W, Kashuba A, Lewin S,

784   Margolis D, Mau M, Ruelas D, Saleh S, Shirakawa K, Siliciano R, Singhania A, Soto P, Terry V, Verdin

785   E, Woelk C, Wooden S, Xing S, Planelles V. 2013. An In-Depth Comparison of Latent HIV-1 Reactivation

786   in Multiple Cell Model Systems and Resting CD4 + T Cells from Aviremic Patients. PLoS Pathog 9:1–

787   15.

788   44.   Vazquez B, Laguna T, Carabana J, Krangel M, Lauzurica P. 2009. CD69 Gene Is Differentially Regulated

789   in T and B Cells by Evolutionary Conserved Promoter-Distal Elements. J Immunol 1–10.

790   45.   Darcis G, Kula A, Bouchat S, Fujinaga K, Corazza F, Ait-Ammar A, Delacourt N, Melard A, Kabeya K,

791   Vanhulle C, Van Driessche B, Gatot JS, Cherrier T, Pianowski L, Gama L, Schwartz C, Vila J, Burny A,

792   Clumeck N, Moutschen M, De Wit S, Peterlin BM, Rouzioux C, Rohr O, Van Lint C. 2015. An In-Depth

793   Comparison of Latency-Reversing Agent Combinations in Various In Vitro and Ex Vivo HIV-1 Latency

794   Models Identified Bryostatin-1+JQ1 and Ingenol-B+JQ1 to Potently Reactivate Viral Gene Expression.

795   PLoS Pathog 11:1–36.

796   46.   Kula A, Delacourt N, Bouchat S, Darcis G, Avettand-Fenoel VV, Verdikt R, Corazza F, Necsoi C,

797   Vanhulle C, Bendoumou M, Burny A, De Wit SS, Rouzioux C, Rohr OO, Van Lint C. 2019.

798   Heterogeneous HIV-1 Reactivation Patterns of Disulfiram and Combined Disulfiram + Romidepsin

799   Treatments. J Acquir Immune Defic Syndr 80:605–613.

800   47.   Ait-Ammar A, Kula A, Darcis G, Verdikt R, De Wit S, Gautier V, Mallon PWG, Marcello A, Rohr O,

801   Van Lint C. 2019. Current Status of Latency Reversing Agents Facing the Heterogeneity of HIV-1 Cellular

802   and Tissue Reservoirs. Front Microbiol 10:3060.

803   48.   Pierard V, Guiguen A, Colin L, Wijmeersch G, Vanhulle C, Van Driessche B, Dekoninck A, Blazkova J,

804   Cardona C, Merimi M, Vierendeel V, Calomme C, Nguyên TL-A, Nuttinck M, Twizere J-C, Kettmann R,

805   Portetelle D, Burny A, Hirsch I, Rohr O, Van Lint C. 2010. DNA cytosine methylation in the bovine

806   leukemia virus promoter is associated with latency in a lymphoma-derived B-cell line: potential

807   involvement of direct inhibition of cAMP-responsive element (CRE)-binding protein/CRE

808   modulator/activation transcription. J Biol Chem 285:19434–49.

809   49.   Patnaik D, Estève P-O, Pradhan S. 2018. Targeting the SET and RING-associated (SRA) domain of

810   ubiquitin-like, PHD and ring finger – containing 1 (UHRF1) for anti-cancer drug development. Oncotarget

811   9:26243–26258.

812   50.   Grunau C, Schattevoy R, Mache N, Rosenthal A. 2000. MethTools : a toolbox to visualize and analyze

813   DNA methylation data. Nucleic Acids Res 28:1053–1058.

814   51.   Dignam JD, Lebovitz RM, Roeder RG. 1983. Accurate transcription initiation by RNA polymerase II in a

815   soluble extract from isolated mammalian nuclei. Nucleic Acids Res 11:1475–1489.

816   52.   Colin L, Vandenhoudt N, de Walque S, van Driessche B, Bergamaschi A, Martinelli V, Cherrier T,

817   Vanhulle C, Guiguen A, David A, Burny A, Herbein G, Pancino G, Rohr O, van Lint C. 2011. The AP-1

818   binding sites located in the pol gene intragenic regulatory region of HIV-1 are important for viral

819   replication. PLoS One 6:1–19.

820   53.   Naldini L, Blomer U, Gallay P, Ory D, Mulligan R, Gage FH, Verma IM, Trono D. 1996. In vivo gene

821   delivery and stable transduction of post mitotic cells by a lentiviral vector. Science (80-) 272:263–267.

822   54.   Marban C, Suzanne S, Dequiedt F, De Walque S, Redel L, Van Lint C, Aunis D, Rohr O. 2007.

823   Recruitment of chromatin-modifying enzymes by CTIP2 promotes HIV-1 transcriptional silencing.

824   EMBO J 26:412–423.

825   55.   Dedeurwaerder S, Defrance M, Bizet M, Calonne E, Bontempi G, Fuks F. 2013. A comprehensive

826   overview of Infinium Human Methylation450 data processing. Brief Bioinform 15:929–941.

827   56.   Dedeurwaerder S, Defrance M, Calonne E. 2011. Evaluation of the Infinium Methylation 450K technology
828   T echnology R eport. Futur Med 3:771–784.

829   57.   Boom R, Sol C, Salimans M, Jansen C, Wertheim-Van Dillen P, Van der Noordaa J. 1990. Rapid and
830   Simple Method for Purification of Nucleic Acids. J Clin Microbiol 28:495–503.

831   58.   Malnati MS, Scarlatti G, Gatto F, Salvatori F, Cassina G, Rutigliano T, Volpi R, Lusso P. 2008. A universal
832   real-time PCR assay for the quantification of group-M HIV-1 proviral load. Nat Protoc 3:1240–1248.

833   59.   Pasternak AO, Jurriaans S, Bakker M, Prins J, Berkhout B, Lukashov V. 2009. Cellular Levels of HIV
834   Unspliced RNA from Patients on Combination Antiretroviral Therapy with Undetectable Plasma Viremia
835   Predict the Therapy Outcome. PLoS One 4.

836   60.   Avettand-Fenoel V, Chaix M-L, Blanche S, Burgard M, Floch C, Toure K, Allemon M-C, Warszawski J,
837   Rouzioux C. 2009. LTR Real-Time PCR for HIV-1 DNA Quantitation in Blood Cells for Early Diagnosis
838   in Infants Born to Seropositive Mothers Treated in HAART Area. J Med Virol 81:217–223.

839   61.   Kuiken C, Leitner T, Foley B, Hahn B, Marx P, McCutchan F, Wolinsky S, Korker Bette. 2008. HIV
840   Sequence Compendium 2008. Los Alamos, New Mexico.

841

842 **TABLE AND FIGURE LEGENDS**

843 **Figure 1: 5-AzadC-induced reactivation of HIV-1 gene expression from latency is associated with**

844 **5'LTR CGIs demethylation.**

845   **(A)** Schematic presentation of the three CpG islands studied along the HIV-1 provirus, in the

846 HIV-1 promoter (5'LTR and NCR CGIs) and in *rev* (ETR CGI). The reactivation of HIV-1 production

847 following 72h treatment with 400nM of 5-AzadC, quantified by ELISA on p24^{Gag} capsid protein in

848 culture supernatants, and the DNA methylation profile, established by sodium bisulfite sequencing for

849 the three CGIs, are respectively presented for the J-Lat 6.3 cells **(B and C)**, the J-Lat 8.4 cells **(D and**

850 **E)**, the J-Lat 9.2 cells **(F and G)** and the J-Lat 15.4 cells **(H and I)**. ELISA results are representative of

851 the means ± SD of three independent 5-AzadC treatments. Folds reactivation are indicated.

852 Unmethylated and methylated CpG dinucleotides are respectively represented with open and closed

853 circles, where each line corresponds to individual sequenced molecules. The global methylation level

854 presented correspond to mean percentages of methylated CpGs for the twelve clones of each condition,

855 either on the promoter CGIs (5'LTR + NCR CGIs considered together) or on the ETR CGI. Statistical

856 significance was determined by unpaired T test.

857

858 **Figure 2: UHRF1 binds *in vitro* to the methylated DDMP5 and *in vivo* to the latent HIV-1**

859 **promoter.**

860   **(A)** The radiolabeled unmethylated or the methylated HIV-1 DDMP5 probe (respectively

861 indicated as "DDMP5" and "DDMP5-me") were incubated with 10μg of nuclear extracts from Jurkat T

862 cells ("Jurkat NE") and either with a purified rabbit IgG as a negative control (lane 3 and lane 9), or

863 with an antibody directed against CREB/CREM family members including CREB (lane 4 and lane 10),

864 CREM (lane 5 and lane 11) or ATF1 (lane 6 and lane 12). The figure shows the specific retarded bands

865 of interest indicated by arrows. Supershifted complexes are indicated by asterisks. One representative

866 experiment out of three is presented. **(B)** The "DDMP5" or "DDMP5-me" probes were incubated with

867 10μg of Jurkat cells NE, and either with purified rabbit IgG as a negative control (lane 5), or with an

868 antibody directed against methylcytosines-recognizing proteins, including MBD2 (lane 6), MBD4 (lane

869 7), Kaiso (lane 8), UHRF1 (lane 9), MeCP2 (lane 10) and RBP-JK (lane 11). The figure shows the

870 specific retarded bands of interest indicated by arrows. Supershifted complexes are indicated by

871 asterisks. One representative experiment out of three is presented. **(C)** Chromatin preparations of J-Lat

872 8.4 cells, either mock-treated or treated with 400nM of 5-AzadC for 72h, were immunoprecipitated with

873 an anti-UHRF1 antibody or with purified rabbit IgG, serving as a negative control. qPCRs were

874 performed with primers hybridizing specifically to the 5'LTR, in the Nuc-1 region. Fold enrichments

875 relative to IgG are presented, where fold enrichments for each immunoprecipitated DNA were calculated

876 by relative standard curve on input DNA. Values represent the means of duplicate samples ± SD.

877 Statistical significance was calculated with an unpaired T test. One representative experiment out of

878 three is presented. **(D)** Chromatin preparation of J-Lat 6.3 cells, J-Lat 9.2 cells and J-Lat 15.4 cells were

26

879   immunoprecipitated with anti-UHRF1 or purified rabbit IgG as a negative control. qPCR were
880   performed with primers hybridizing specifically to the 5'LTR, in the Nuc-1 region. Fold enrichments
881   relative to IgG are presented, where fold enrichments for each immunoprecipitated DNA was calculated
882   by relative standard curve on input DNA. Values represent the means ± S.D of one representative
883   experiment out of three. (E) Spearman correlation was calculated between the percentage of methylation
884   on DDMP5 and UHRF1 recruitment fold specific to the HIV-1 promoter, based on dataset from Figure
885   1, Figure 2C and Figure 2D.

886

887   **Figure 3: UHRF1 silencing of HIV-1 transcription is dependent on 5'LTR methylation.**
888   (**A**) Chromatin was prepared from J-Lat 8.4 cells, either mock-transduced, control-transduced (with non-
889   targeting shRNA, indicated as "shNT-transduced") or shUHRF1-transduced (indicated as "shUHRF1-
890   transduced"). Immunoprecipitations were performed using anti-RNAPII or purified rabbit IgG, as a
891   negative control. qPCRs were performed with primers hybridizing specifically to the 5'LTR, in the Nuc-
892   1 region. Fold enrichments relative to IgG are presented, where fold enrichments for each
893   immunoprecipitated DNA were calculated by relative standard curve on input DNA. Values represent
894   the means of duplicate samples ± SD. (**B**) Total RNA preparations from mock-transduced, shNT-
895   transduced or shUHRF1-transduced J-Lat 8.4 cells were reverse transcribed. Initiated (TAR region),
896   elongated (*tat* region) transcripts, or HIV-1 multiple-spliced RNA (MS RNA) were quantified by RT-
897   qPCR using GAPDH as first normalizer and the mock-transduced condition as second normalizer.
898   Means from duplicate ± SD are indicated. (**C**) Cultures supernatants from mock-transduced, shNT-
899   transduced or shUHRF1-transduced J-Lat 8.4 cells were probed for viral production as measured by
900   ELISA on p24^{Gag} capsid protein. (**D**) DNA methylation mapping performed by sodium bisulfite
901   sequencing is presented for the promoter CGIs or the intragenic ETR CGI in J-Lat 8.4 cells mock-
902   transduced, shNT-transduced or shUHRF1-transduced, as indicated. Unmethylated and methylated CpG
903   dinucleotides are respectively represented with open and closed circles, where each line corresponds to
904   individual sequenced molecules. The global methylation level presented correspond to mean
905   percentages of methylated CpGs for the twelve clones of each condition, either for the promoter CGIs
906   considered together (5'LTR + NCR CGIs) or for the ETR CGI. Panel A to D originate from the same
907   representative experiment out of three. (**E**) Chromatin was prepared from J-Lat 8.4 cells, either mock-
908   transduced or shUHRF1-transduced. Immunoprecipitations were performed using anti-DNMT1, anti-
909   G9a or purified rabbit IgG, as a negative control. qPCRs were performed with primers hybridizing
910   specifically to the 5'LTR, in the Nuc-1 region. Fold enrichments relative to IgG are presented, where
911   fold enrichments for each immunoprecipitated DNA were calculated by relative standard curve on input
912   DNA. Values represent the means of duplicate samples ± SD. (**F**) HEK293T cells were transfected either
913   with 600ng of the pshNT vector or with 600ng of the pshUHRF1#4. Twenty-four hours after this initial
914   transfection, 400ng of the pLTR-Fluc, the pLTRme-Fluc or the pLTR'Cpg5me)-Fluc reporter constructs
915   together with or without 200ng of the plasmid overexpressing UHRF1 (pUHRF1) were co-transfected.

27

916   Luciferase activities were measured in the cell lysates after further 24h post-transfection. Results are

917   presented as histograms of "relative luciferase units" (R.L.U.), corresponding to the Fluc activiy

918   normalized to the total levels of proteins. Means and standard errors of triplicate samples are

919   represented. An experiment representative of three independent experiments is shown. Statistical

920   significance was assessed by an unpaired T test. **(G)** UHRF1 and β-actin, serving as a loading control,

921   protein levels were assessed by immunoblot in cell lysates of the corresponding transfection points.

922

923   **Figure 4: HIV-1 transcription is reactivated from latency upon UHRF1 downregulation by**

924   **epigallo-catechin-3-gallate.**

925   **(A)** Total RNA preparations from J-Lat 8.4 cells mock-treated or treated with increasing doses of

926   EGCG for 24h were used in RT-qPCR to quantify initiated (TAR region), *gag*, elongated (*tat* region)

927   transcripts, or HIV-1 MS RNA, using GAPDH as normalizer. **(B)** After 24h of EGCG increasing doses

928   treatment, J-Lat 8.4 cells were analyzed by flow cytometry to quantify the percentage of GFP+ cells.

929   **(C)** WST-1 proliferation assay, reflective of metabolic activity, was performed on J-Lat 8.4 cells treated

930   for 24h with increasing doses of EGCG. The result obtained with mock-treated cells was set a value of

931   100%. A, B and C originate from the same representative experiment out of three. Means ± SD of

932   duplicates are presented. Statistical significance was calculated with an unpaired T test and corresponds

933   to comparisons to the mock-treated condition. **(D)** J-Lat 8.4 cells, either mock-transduced or shUHRF1-

934   transduced were treated for 24h with 70μg/mL of EGCG. The percentage of GFP positive cells was

935   assessed by flow cytometry and was normalized to the respective mock conditions. Means ± SD of

936   duplicates representative of three independent experiments are presented. Statistical significance was

937   assessed by an unpaired T test. **(E)** Whole protein levels of the experiments presented in Fig. 4D were

938   loaded and probed for the presence of UHRF1 and and β-actin, serving as a loading control. **(F)**

939   Quantification of the western blot presented in Fig. 4E was performed in ImageJ. Means ± SD of two

940   independent quantifications are presented. Statistical significance was assessed by an unpaired T test.

941   **(G)** An Infinium assay with gDNA from above was conducted. Differential methylated CpGs upon

942   EGCG treatment were plotted on a pie chart, where the black slice represents hypermethylated CpGs

943   and the white slice represents hypomethylated CpGs. **(H)**) An Infinium assay with gDNA from Fig. 3

944   was conducted. Differential methylated CpGs upon shUHRF1 transduction were plotted on a pie chart,

945   where the black slice represents hypermethylated CpGs and the white slice represents hypomethylated

946   CpGs. **(I)** Venn diagram representing the number of hypomethylated CpGs in both conditions is

947   presented.

948

949   **Figure 5: EGCG reactivates the expression of viral RNA in *ex vivo* cultures of CD8^{+}-depleted**

950   **PBMCs isolated from cART-treated aviremic HIV-1+ individuals.**

951   *Ex vivo* cultures of CD8^{+}-depleted PBMCs isolated from 22 cART-treated aviremic HIV^{+} individuals

952   were mock-treated or treated for 24h with EGCG, at the indicated concentrations, or with anti-

28

953 CD3+anti-CD28 antibodies serving as positive control stimulation. **(A)** Total intracellular RNA was
954 extracted and cell-associated HIV-1 US RNA was quantified. Medians are represented. Open circles
955 depict undetectable values, censored to the assay detection limits. The latter depended on the amounts
956 of input cellular RNA and therefore differed between samples. Statistical significance was determined
957 by paired Wilcoxon tests, where pairs were included in the analysis only when either (i) both values in
958 a pair were detectable, or (ii) one value in a pair was undetectable and the other detectable, and the
959 maximal value of the undetectable (the assay detection limit) was lower than the detectable. **(B)** In 7 out
960 of 22 HIV[+] individuals, the concentration of HIV-1 extracellular genomic RNA in culture supernatants
961 was also determined (in copies/ml).

962

963 **Table 1: Most statistically significant 5-AzadC-induced differentially-demethylated CpG**
964 **dinucleotides (DDMPs).**
965 [a] Position given in coordinates where nt+1 is located at the junction U3/R in the 5'LTR.
966 [b] Statistical significance attributed with * for $p \leq 0.05$, ** for $p \leq 0.01$ and *** for $p \leq 0.001$ by Fisher's
967 exact test.
968 [c] Location of CpG within regulatory or structural elements according to the HIV-1 Database (19, 61).
969 N/A refers to no known features.
970 [d] Differentially-Demethylated Position.
971 DDMPs located in transcription factor binding sites are in bold.

972

973 **Figure S1: Mapping of 5-AzadC-induced demethylation probability reveals hotspots of**
974 **demethylation.**
975 **(A)** Schematic view of CpG dinucleotides position in the 5'LTR and transcription factor binding sites
976 positions. The individual probabilities of 5-AzadC-induced demethylation at each CpG dinucleotide,
977 presented in histograms on the left Y axis and associated p-values (Fisher's exact test), presented in blue
978 on the right Y axis, was calculated in J-Lat 6.3 cells **(B)**, in J-Lat 8.4 cells **(C)**, in J-Lat 9.2 cells **(D)** and
979 in J-Lat 15.4 cells **(E)** using the data presented in Figure 1. Statistically significant DDMPs located in
980 transcription factor binding sites are highlighted and indicated by an arrow.

981

982 **Figure S2: Methylation of DDMP5 promotes the sequence-specific and methylation-specific *in***
983 ***vitro* binding of an additional factor.**
984 **(A)** The radiolabeled unmethylated or methylated HIV-1 DDMP5 probe was incubated with 10µg
985 of Jurkat cells NE, in the absence of competitor, or in presence of increasing molar excesses of the
986 unlabeled homologous, respectively methylated (lanes 7-9 and lanes 11-13) or unmethylated (lanes 3-5
987 and lanes 15-17), HIV-1 DDMP5 oligonucleotides. **(B)** The quantification of the band corresponding to
988 the C1 complex for the competition with the unmethylated competitor (equivalent to the lanes 3-5) and
989 the methylated competitor (equivalent to the lanes 7-9) is presented. Statistical significance was

29

990   calculated by an unpaired T test. **(C)** The methylated HIV-1 DDMP5 radiolabeled probe was incubated

991   with 10µg of Jurkat NE, in the absence of competitor, or in presence of increasing molar excesses of the

992   heterologous unlabeled methylated MBD consensus (indicated as "MBD-me", lanes 3-5)) or methylated

993   Sp1 consensus (indicated as "Sp1-me", lanes 7-10) oligonucleotides. Binding reactions were analyzed

994   by PAGE, and retarded complexes were visualized by autoradiography. The major DNA-protein

995   complexes C1 and C2 are indicated by arrows. The figure shows only the specific retarded bands of

996   interest. One representative experiment out of three is presented.

997

998   **Figure S3: UHRF1 expression is not affected by 5-AzadC.**

999   **(A)** Total RNA preparations from the J-Lat 8.4 cells, either mock-treated or treated with 400nM

1000   of 5-AzadC for 72h were reverse transcribed. UHRF1 transcripts were quantified by reverse

1001   transcription qPCR using GAPDH as a normalizer. Means from duplicates ± SD are indicated. Statistical

1002   significance was calculated with an unpaired T test. One representative experiment out of three is

1003   presented. **(B)** Total protein extracts from the same stimulation as in (D) were extracted. UHRF1 was

1004   immunodetected by western blotting using a specific antibody. Levels of β-actin were measured to

1005   control protein loading. One representative experiment out of three is presented.

1006

1007   **Figure S4: UHRF1 depletion in J-Lat 8.4 cells following shUHRF1 transduction provokes**

1008   **reactivation of HIV-1 and specific demethylation patterns in the viral promoter.**

1009   **(A)** UHRF1 and β-actin, serving as a loading control, protein levels were assessed by immunoblot

1010   in whole-cell lysates of J-Lat 8.4 cells mock-transduced, transduced with a control shRNA (indicated as

1011   "shNT-transduced") or transduced with four independent shUHRF1 (indicated as "shUHRF1#1-4-

1012   transduced"). **(B)** Total RNA preparations were used in RT-qPCR to quantify UHRF1 transcripts, using

1013   GAPDH as a first normalizer and the mock-transduced condition as second normalizer. Values

1014   correspond to means ± SD of two independent qPCRs. **(C)** The quantity of p24^{Gag} in the culture

1015   supernatants was evaluated by ELISA. Results are representative of the mean ± SD two independent

1016   ELISA quantifications. The whole panel originates from one representative experiment out of three.

1017   Statistical significance was assessed by an unpaired T test and corresponds, if not otherwise specified,

1018   to comparisons to the mock-transduced condition. **(D)** Schematic view of CpG dinucleotides position in

1019   5'LTR and transcription factor binding sites positions. The individual probabilities of 5-AzadC-induced

1020   demethylation at each CpG dinucleotide, presented in histograms on the left Y axis and associated p-

1021   values (Fisher's exact test), presented in blue on the right Y axis, was calculated in J-Lat 8.4 cells shNT-

1022   transduced in comparison to mock-transduced cells **(E)**, in J-Lat 8.4 cells shUHRF1-transduced in

1023   comparison to shNT-transduced cells **(F)** and in in J-Lat 8.4 cells shUHRF1-transduced in comparison

1024   to mock-transduced cells **(G)**, using the data presented in Figure 3. Statistically significant DDMPs

1025   located in transcription factor binding sites are highlighted.

1026

1027 **Figure S5: UHRF1 is downregulated in J-Lat 8.4 cells following EGCG treatment.**

1028 **(A)** UHRF1 and β-actin, serving as a loading control, protein levels were assessed by immunoblot in
1029 whole-cell lysates of J-Lat 8.4 cells mock-treated or treated with increasing doses of EGCG for 24h. **(B)**
1030 Total RNA preparations from the same experiment as in A were used in RT-qPCR to quantify UHRF1
1031 transcripts, using GAPDH as a first normalizer and the mock-treated condition as second normalizer.
1032 One representative experiment is shown out of three. Statistical significance was assessed using an
1033 unpaired T test. **(C)** The quantity of p24^{Gag} in the culture supernatants of mock-treated or EGCG-treated
1034 J-Lat 8.4 cells was evaluated by ELISA. Results are representative of the mean ± SD of three
1035 independent EGCG treatment. The limit of the test detection at 10pg/mL is indicated. Statistical
1036 significance was assessed using an unpaired T test.

1037

1038 **Figure S6: Methylome-wide analyses of shUHRF1 and EGCG-induced hypomethylation show**
1039 **different patterns.**

1040 **(A)** Hierarchical clustering was performed on the most variable CpGs obtained in the Infinium
1041 assay for the genomic DNA samples of Fig. 3 and Fig. 4. **(B)** Principal component analysis was
1042 performed on the most variable CpGs obtained in the Infinium assay for the genomic DNA samples of
1043 Fig. 3 and Fig. 4. **(C)** Enriched pathways corresponding to the differential DNA methylation profile
1044 upon EGCG treatment were analyzed by GSEA. Grey bars represent non-significant pathways, purple
1045 bars represent statistically significative common pathways and white bars represent statistically
1046 significative but not common pathways. **(D)** Enriched pathways corresponding to the differential DNA
1047 methylation profile upon shUHRF1 transduction were analyzed by GSEA.

1048

1049 **Figure S7: Effects of EGCG on cellular viability, metabolic activity, cell surface activation**
1050 **markers and CD4 expression in CD8^{+}-depleted PBMCs from healthy donors.**

1051 CD8^{+}-depleted PBMCs were extracted from six healthy donors blood samples and were mock-
1052 treated or treated for 24h with the indicated doses of EGCG, or with anti-CD3+anti-CD28 antibodies
1053 serving as positive control stimulation. **(A)** Cells were stained for CD4+ and LIVE/DEAD Fixable Near-
1054 IR Dead Cell Stain to discriminate between viable and non-viable cells. Medians percentages are
1055 indicated. **(B)** WST-1 proliferation assay, reflective of metabolic activity, was performed on the cells.
1056 Median percentages are indicated. HLA-DR **(C)**, CD25 **(D)**, CD69 **(E)** and CD38 **(F)** expression was
1057 analyzed by flow cytometry. Results are presented as percentage of marker expression in alive CD4+-
1058 gated cell populations. Medians for each condition are presented. **(G)** Mean fluorescence intensify (MFI)
1059 associated with CD4 serves as a surrogate for CD4 surface expression. Medians for each condition are
1060 presented. Statistical significance was calculated by paired comparisons between each treated condition
1061 (Wilcoxon test).

1062

1063

31

1064 **Figure S8: HIV-1 proviruses are statistically more transcriptionally active in EGCG-treated *ex***
1065 ***vivo* patient cell cultures.**

1066 **(A)** Comparison of HIV-1 intracellular US RNA/DNA ratios between mock-treated, EGCG
1067 50μg/mL, EGCG 70μg/mL and positive control stimulations of *ex vivo* patient X15 to X22 cultures is
1068 presented. **(B)** Comparison of HIV-1 extracellular RNA/DNA ratios between mock-treated, EGCG
1069 50μg/mL, EGCG 70μg/mL and positive control stimulations of *ex vivo* patient X15 to X22 cultures is
1070 presented. In both panels, statistical significance was calculated by paired comparisons between each
1071 treated condition (Wilcoxon test). **(C)** The ratios of HIV intracellular US RNA/DNA or extracellular
1072 RNA/DNA were calculated for the individuals X15 to X22. Of note, individual X20 was excluded due
1073 to high level of extracellular HIV-1 RNA in mock-treated condition at 24h post-stimulation.
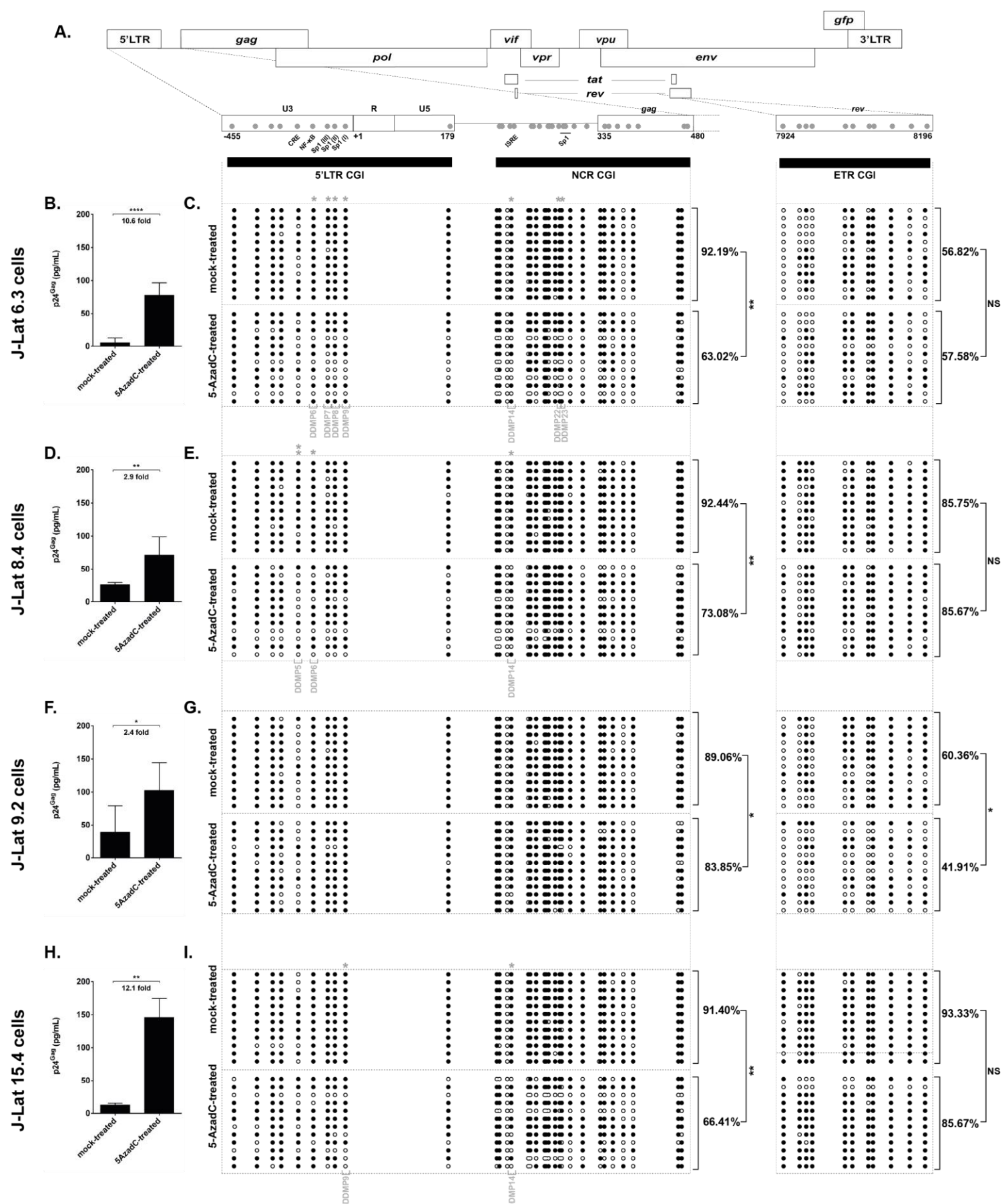
1074 **Figure S9: EGCG reactivation potency *ex vivo* correlates to temporal parameters of infection in**
1075 **HIV+ individuals and follows the DNA methylation level of the viral promoter.**

1076 For HIV+ individuals presenting detectable values of cell-associated HIV-1 US RNA, fold inductions
1077 over mock condition were calculated, based on the data presented in Fig. 5A. Spearman correlations
1078 between quantity of cell-associated HIV-1 US RNA for 50μg/mL of EGCG and time of treatment **(A)**
1079 or time as aviremic **(B)** were calculated based on the data presented in Table S1. In **(C)**, raw values of
1080 Spearman ρ and associate p-values for each condition are presented. **(D)**The methylation status for 8
1081 individuals out of 22 was obtained by sodium bisulfite sequencing. We clustered individuals in groups
1082 presenting non-methylated or methylated 5'LTR and analyzed their respective median EGCG
1083 reactivation capacity, in terms of cell-associated HIV-1 US RNA for 50μg/mL of EGCG.
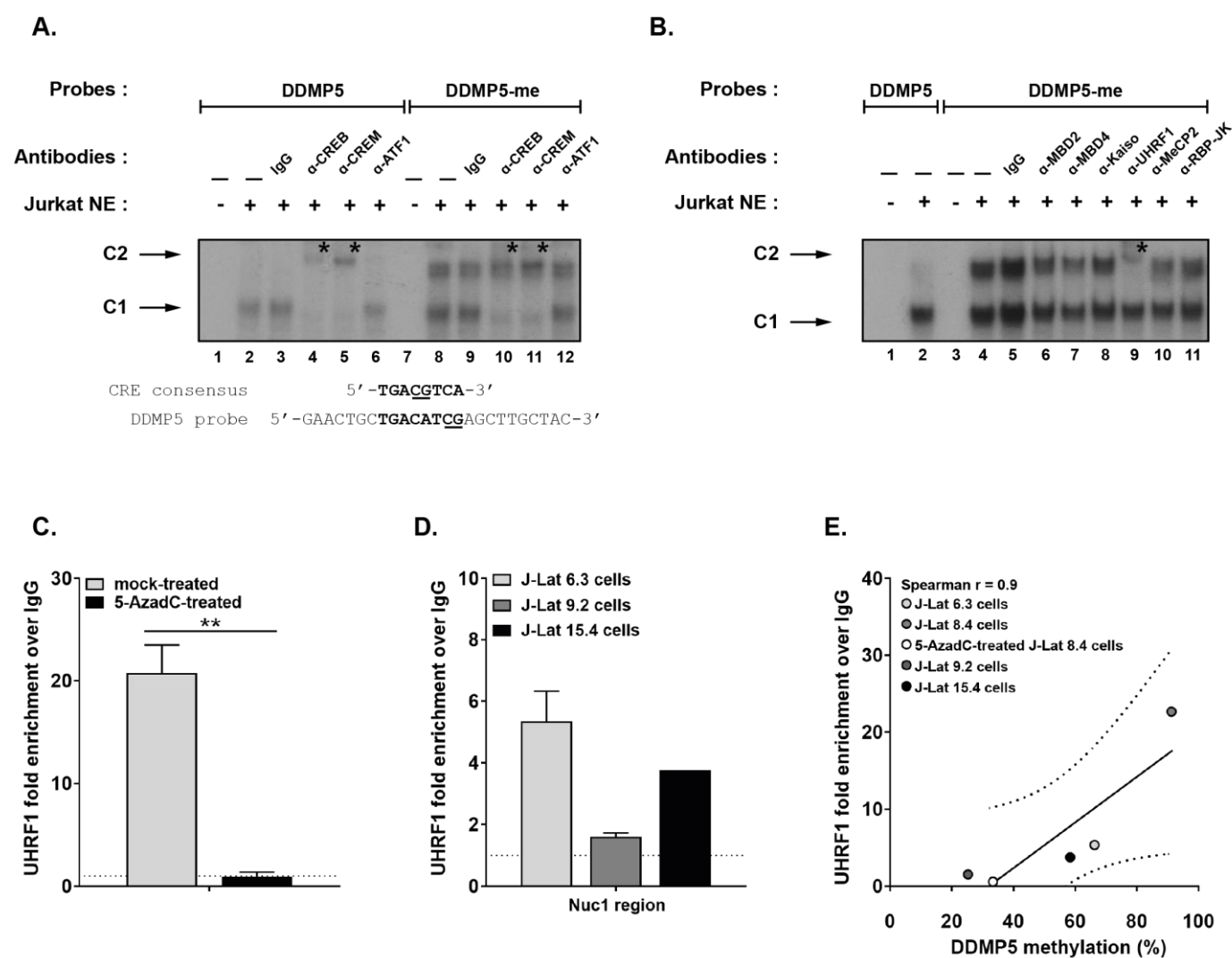
1084

1085 **Table S1: EGCG induces HIV-1 recovery in CD8+-depleted PBMCs from aviremic cART-treated**
1086 **HIV+ individuals**

1087 **(A)** HIV+ individuals' clinical characteristics are listed. ART= antiretroviral therapy, ATV= atazanavir,
1088 DRV= darunavir, DTG= dolutegravir EFV= efavirenz, EVP= eviplera (rilpivirine, emtricitabine,
1089 tenofovir), GENVOYA= elvitegravir/cobicistat/emtricitabine/tenofovir, KVX = kivexa, NPV =
1090 nevirapine, RTV = ritonavir, RPV=rilpivirine, STB = elvitegravir, cobicistat, emtricitabine, tenofovir,
1091 TRI= triple cocktail, TRU = Truvada and "?" = unknown. **(B)** *Ex vivo* cultures of CD8+-depleted PBMCs
1092 purified from blood of 22 aviremic cART-treated HIV+ individuals were mock-treated or treated with
1093 anti-CD3+anti-CD28 antibodies, as positive control stimulation, or with EGCG 50μg/mL or EGCG
1094 70μg/mL. Twenty-four hours or six days post-treatment, concentrations of intracellular unspliced HIV-
1095 1 RNA or of extracellular HIV-1 RNA was determined, respectively in cells and in cell culture
1096 supernatants. Total HIV-1 DNA was expressed as HIV-1 DNA copies *per* million CD8+-depleted
1097 PBMCs. 'I' indicates that the value is below the limit of detection. 'X' indicates that the condition was
1098 not tested. Of note, individual X20 was excluded from extracellular quantification due to high level of
1099 extracellular HIV-1 RNA in mock-treated condition at 24h post-stimulation.
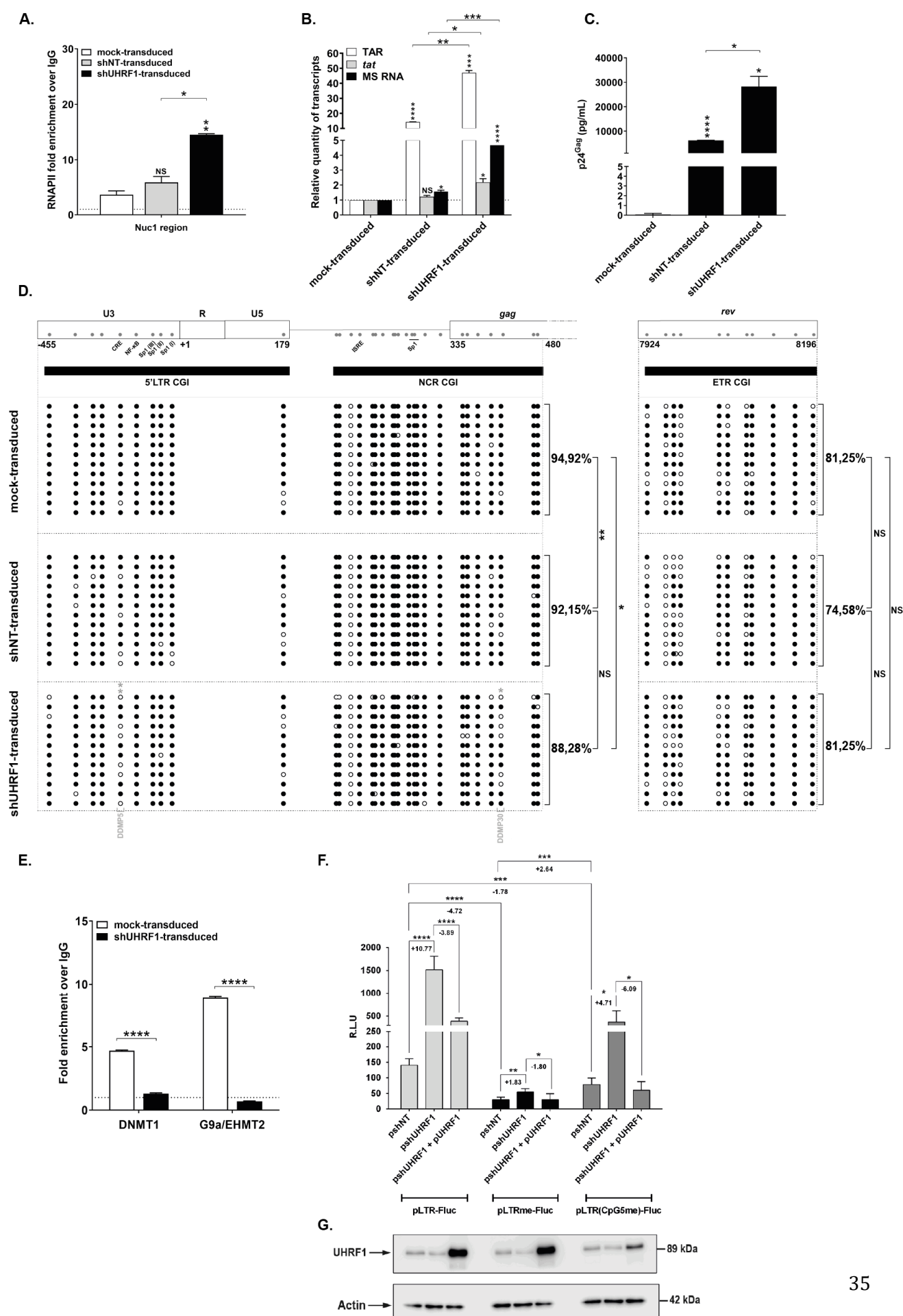
Figure 1

1101   **Figure 2**

CRE consensus   5'-**TGA<u>CG</u>TCA**-3'

DDMP5 probe   5'-GAACTGC**TGACAT<u>CG</u>**AGCTTGCTAC-3'

1102   **Figure 3**

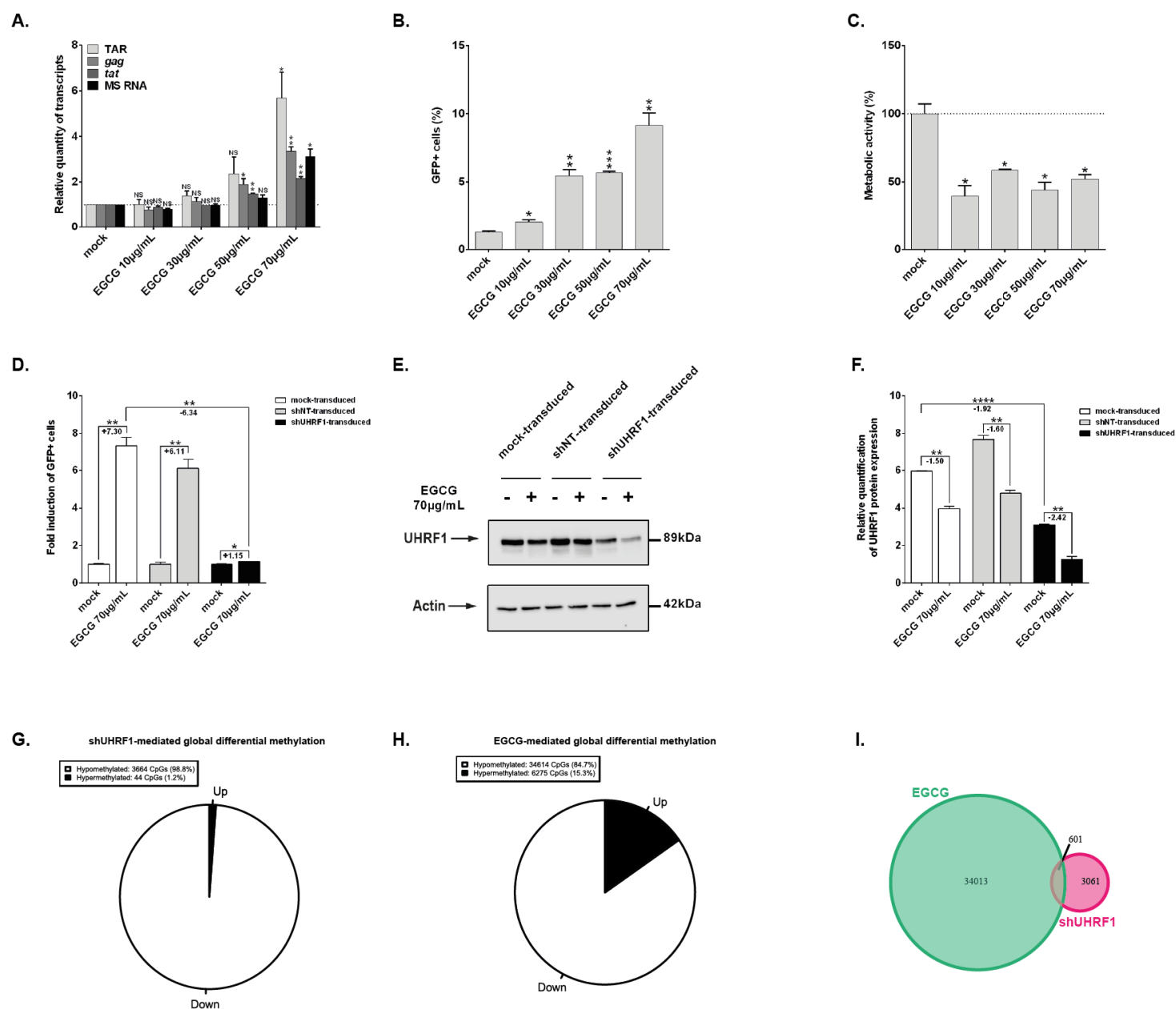1103 **Figure 4**

Figure 5

A.

B.
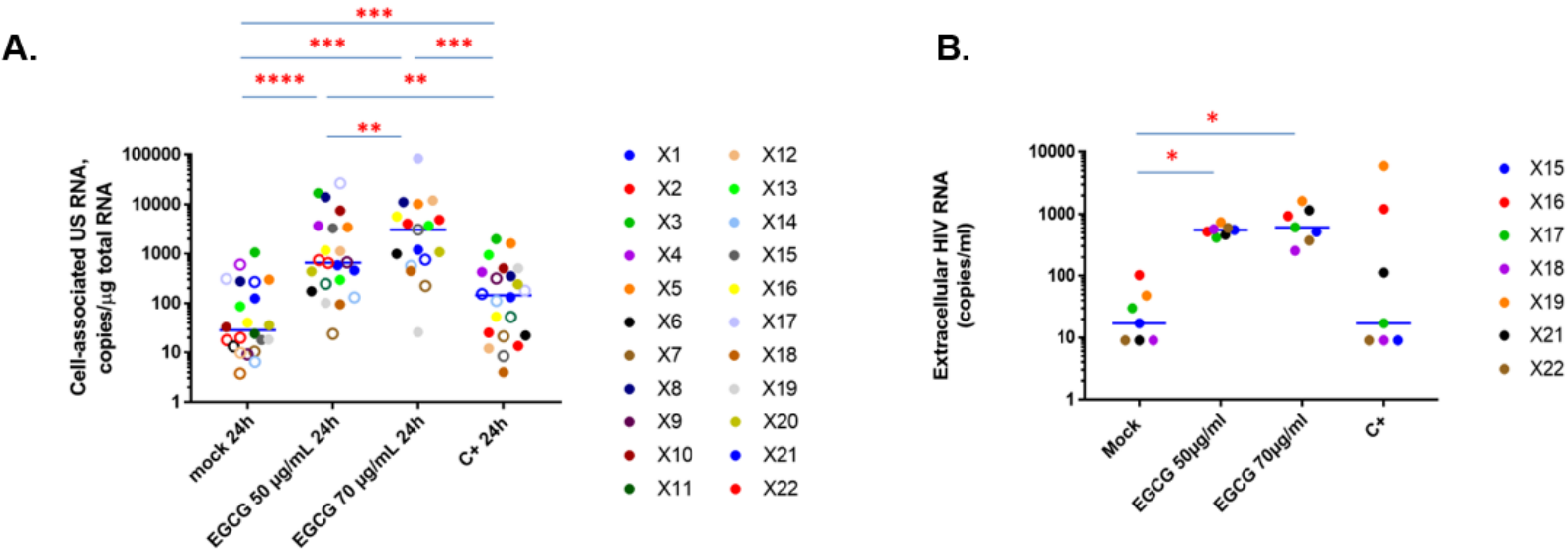
Table 1

Cell line	CpG position[a]	Probability of 5-AzadC-induced demethylation	p-value[b]	Statistical-significance	Location[c]	DDMP[d]
J-Lat 6.3 cells	-[158,159]	0,33	0,046	*	N/A	DDMP3
	-[96, 97]	**0,33**	**0,0466**	*	**NF-κB site**	**DDMP6**
	-[74,75]	**0,45**	**0,32**	*	**Sp1 site III**	**DDMP7**
	-[63,64]	**0,42**	**0,0186**	*	**Sp1 site II**	**DDMP8**
	-[47, 48]	**0,42**	**0,0186**	*	**Sp1 site I**	**DDMP9**
	+[109, 110]	0,42	0,0186	*	U5 interacting with ψ	DDMP10
	+[183, 184]	0,42	0,0186	*	PBS	DDMP11
	+[186, 187]	0,33	0,0466	*	PBS	DDMP12
	+[205, 206]	**0,42**	**0,0186**	*	**Interferon-Stimulated Response Element**	**DDMP14**
	+[243, 244]	0,33	0,0466	*	Zinc Knuckles in p7Gag binding to SL1	DDMP17
	+[261, 262]	0,42	0,0186	*	SL2 of ψ	DDMP20
	+[278, 279]	**0,42**	**0,0186**	*	**Sp1 site of HSIV**	**DDMP22**
	+[282, 283]	**0,33**	**0,0466**	*	**Sp1 site of HSIV**	**DDMP23**
	+[295, 296]	0,33	0,0466	*	SL2 of ψ	DDMP24
	+[314, 315]	0,42	0,0186	*	SL3 of ψ	DDMP25
	+[341, 342]	0,5	0,0069	**	SL4 of ψ	DDMP26
	+[360, 361]	0,33	0,0466	*	Coding sequence of p17Gag	DDMP28
	+[390, 391]	0,6	0,0167	*	Coding sequence of p17Gag	DDMP30
J-Lat 8.4 cells	**-[119, 120]**	**0.64**	**0.0045**	**	**CRE site**	**DDMP5**
	-[96, 97]	**0.33**	**0.0466**	*	**NF-κB site**	**DDMP6**
	+[183, 184]	0.33	0.0466	*	N/A	DDMP11
	+[205, 206]	**0.33**	**0.0466**	*	**Interferon-Stimulated Response Element**	**DDMP14**
	+[231, 232]	0.45	0.0320	*	N/A	DDMP15
	+[360, 361]	0.33	0.0466	*	Coding sequence of p17Gag	DDMP28
J-Lat 15.4 cells	-[217, 218]	0.33	0.0466	*	N/A	DDMP1
	-[47, 48]	**0.42**	**0.0186**	*	**Sp1 site**	**DDMP9**
	+[109, 110]	0.33	0.0466	*	U5 interacting with ψ	DDMP10
	+[205, 206]	**0.42**	**0.0186**	*	**Interferon-Stimulated Response Element**	**DDMP14**
	+[231, 232]	0.42	0.0186	*	N/A	DDMP15
	+[234, 235]	0.33	0.0466	*	SL1 of ψ	DDMP16
	+[243, 244]	0.33	0.0466	*	Zinc Knuckles in p7[Gag] binding to SL1	DDMP17
	+[295, 296]	0.50	0.0069	*	SL2 of ψ	DDMP24
	+[314, 315]	0.33	0.0466	*	SL3 of ψ	DDMP25
	+[341, 342]	0.42	0.0186	*	SL4 of ψ	DDMP26
	+[347, 348]	0.33	0.0466	*	SL4 of ψ	DDMP27
	+[360, 361]	0.36	0.0129	*	Coding sequence of p17Gag	DDMP28

Figure S1

Figure S2

A.

B.

C.

Figure S3

A.

B.
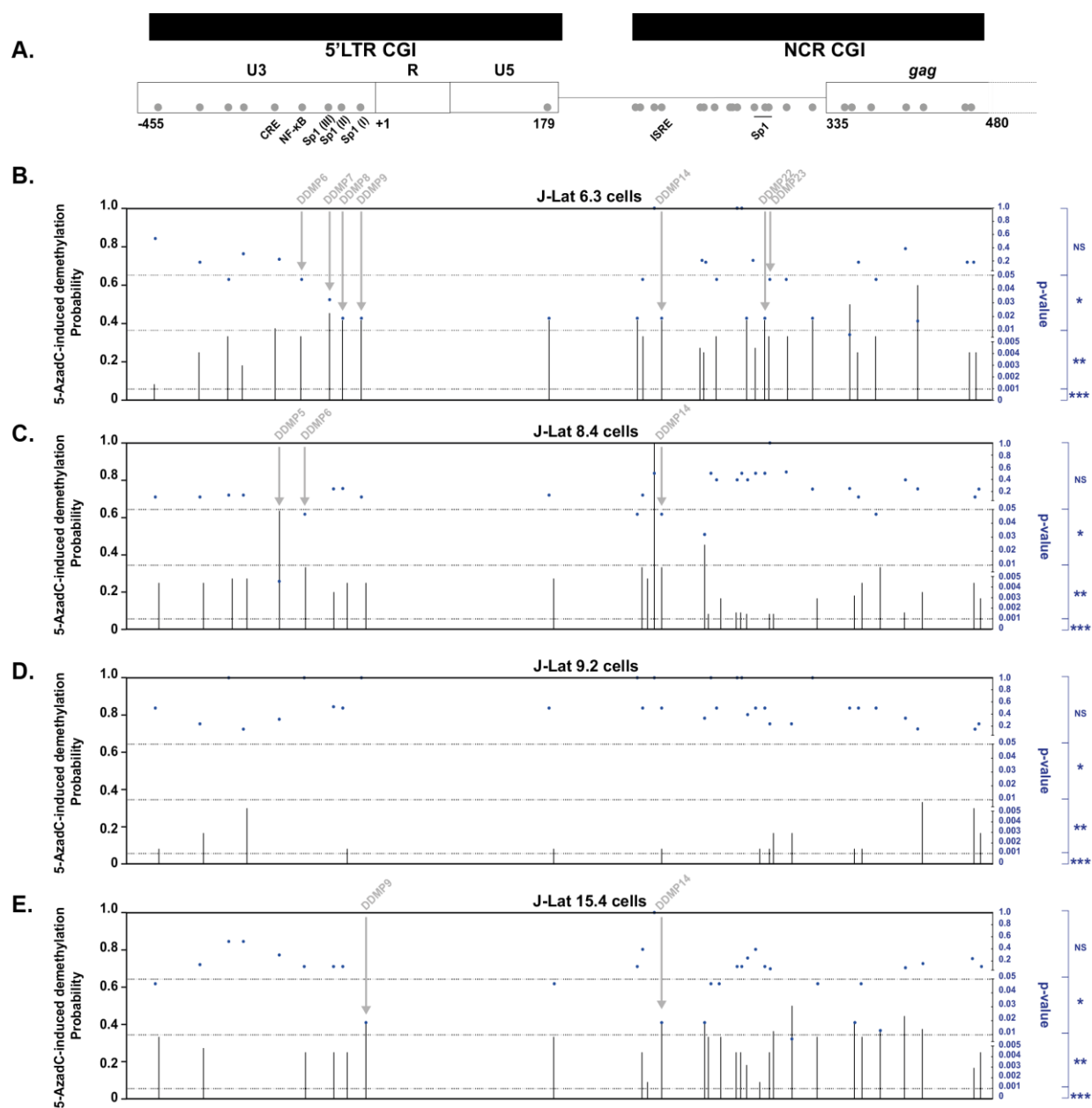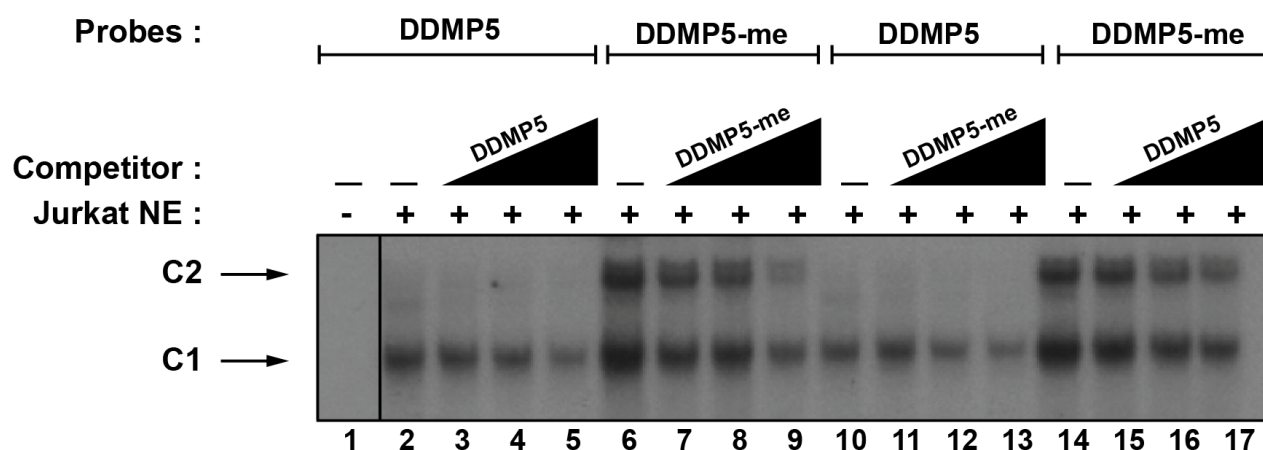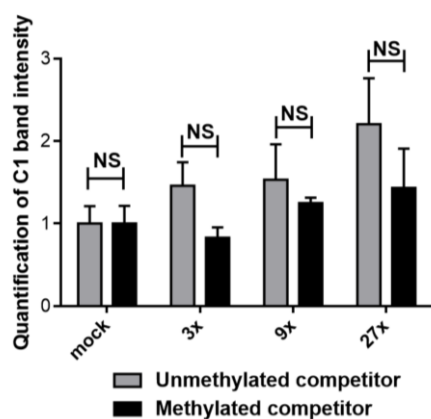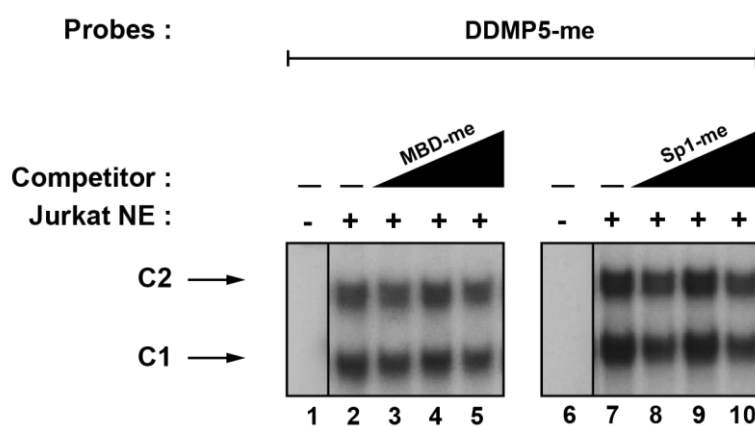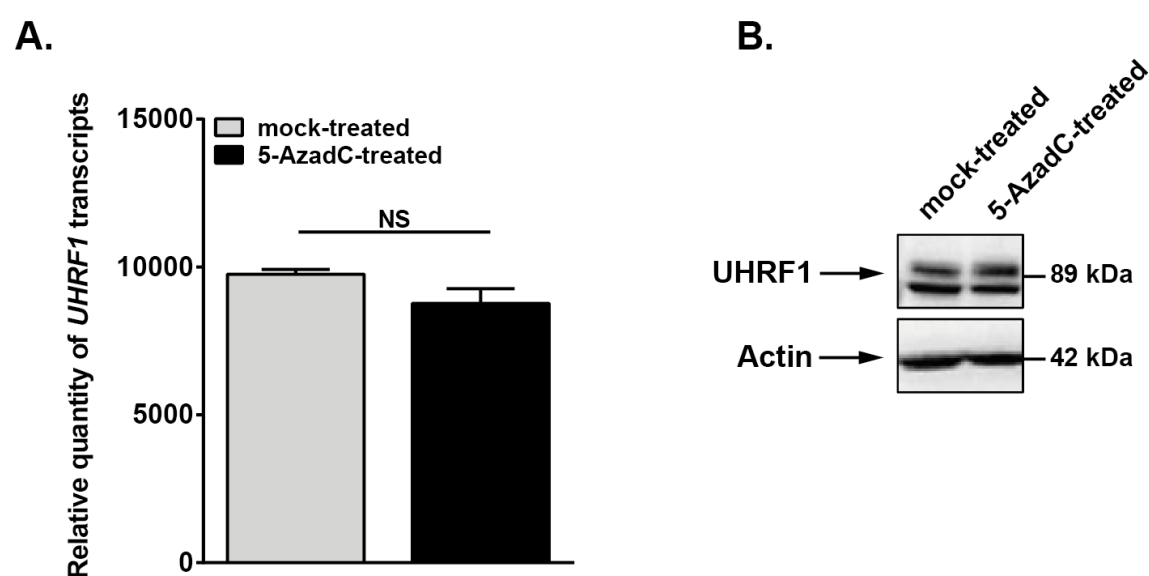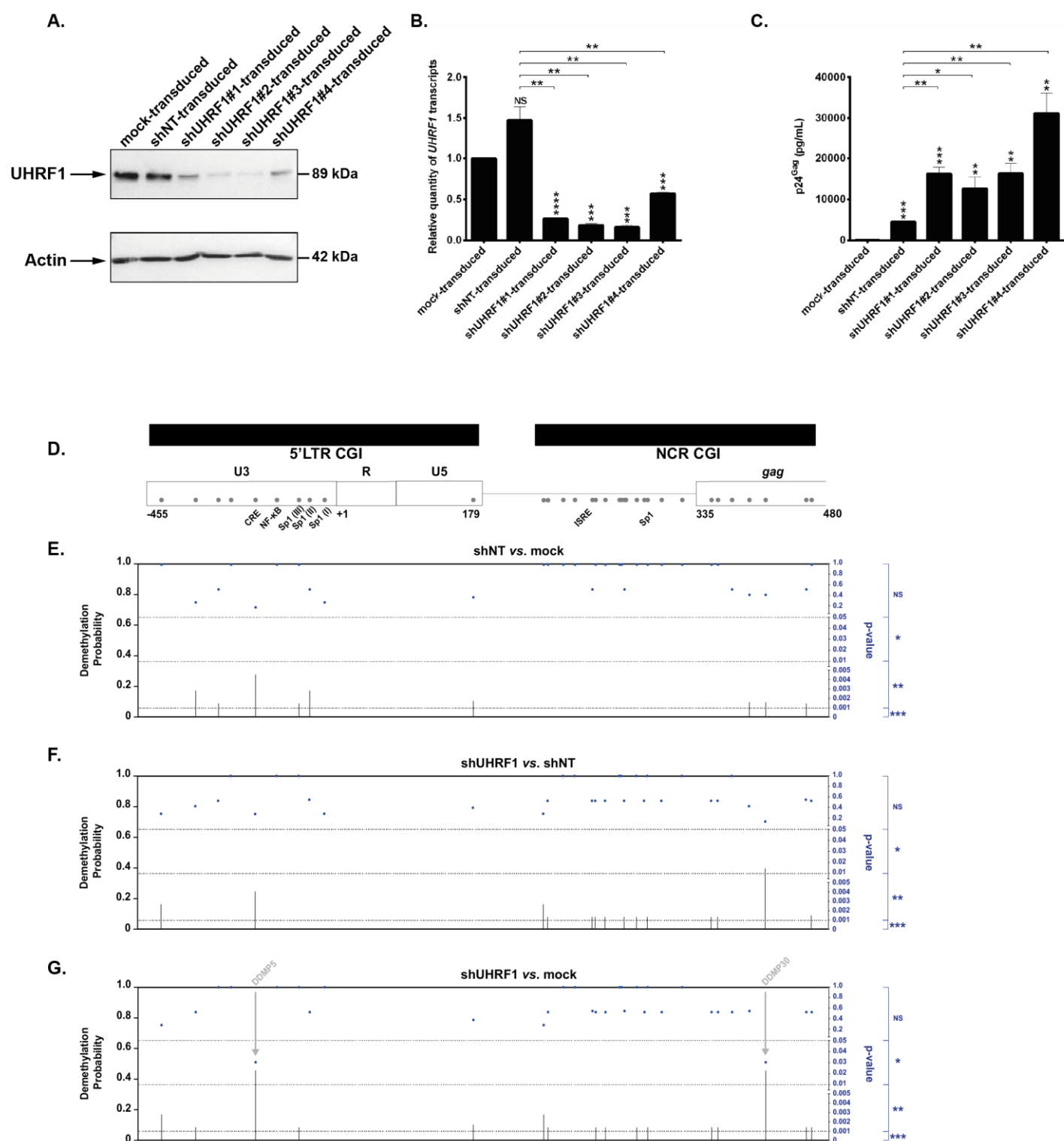
Figure S4

Figure S5
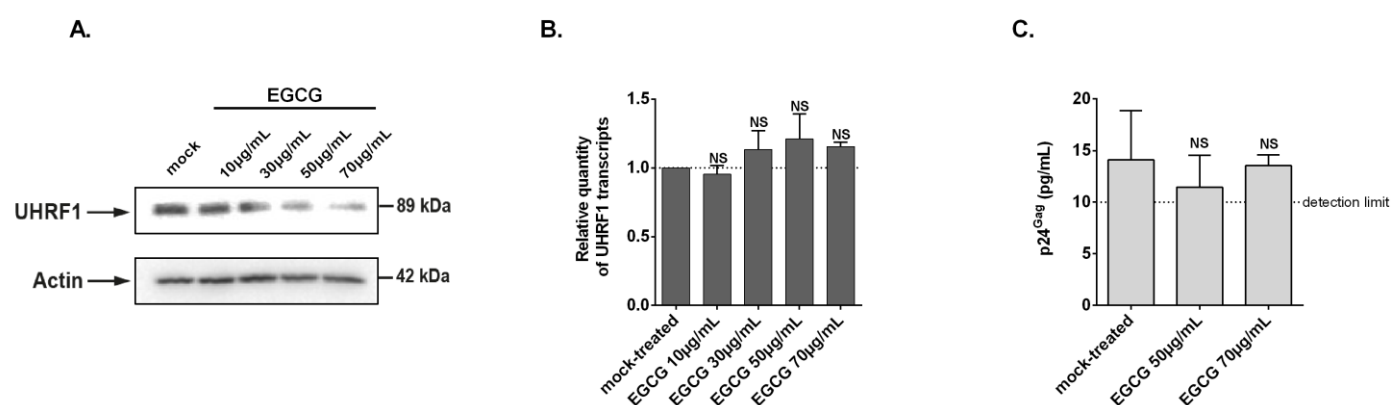
Figure S6

Figure S7

Figure S8

C.

Patient	HIV Intracellular US RNA/DNA				HIV extracellular RNA/DNA			
	Mock	EGCG 50µg/mL	EGCG 70µg/mL	C+	Mock	EGCG 50µg/mL	EGCG 70µg/mL	C+
X15	0,02	4,60	4,32	0,01	0,02	0,77	0,72	0,01
X16	0,03	0,81	3,94	0,04	0,07	0,36	0,64	0,83
X17	0,36	31,03	96,67	0,21	0,03	0,48	0,70	0,02
X18	0,02	0,58	2,75	0,02	0,06	3,49	1,56	0,06
X19	0,02	0,13	0,03	0,66	0,06	0,96	2,13	7,80
X20	0,10	1,27	3,11	0,70	10,40	1,54	4,59	0,55
X21	0,45	2,09	4,29	0,48	0,03	1,65	4,11	0,40
X22	0,02	0,57	4,32	0,02	0,01	0,53	0,33	0,01

Figure S9

A.

B.

C.

	C+ vs. mock		EGCG 50µg/mL vs. mock		EGCG 70µg/mL vs. mock	
	Spearman ρ	p-value	Spearman ρ	p-value	Spearman ρ	p-value
Time on cART	0.21	0.49	0.72	0.0036 **	0.58	0.037*
Time of HIV suppression	0.05	0.84	0.57	0.020*	0.55	0.040*

D.

Table S1

A.

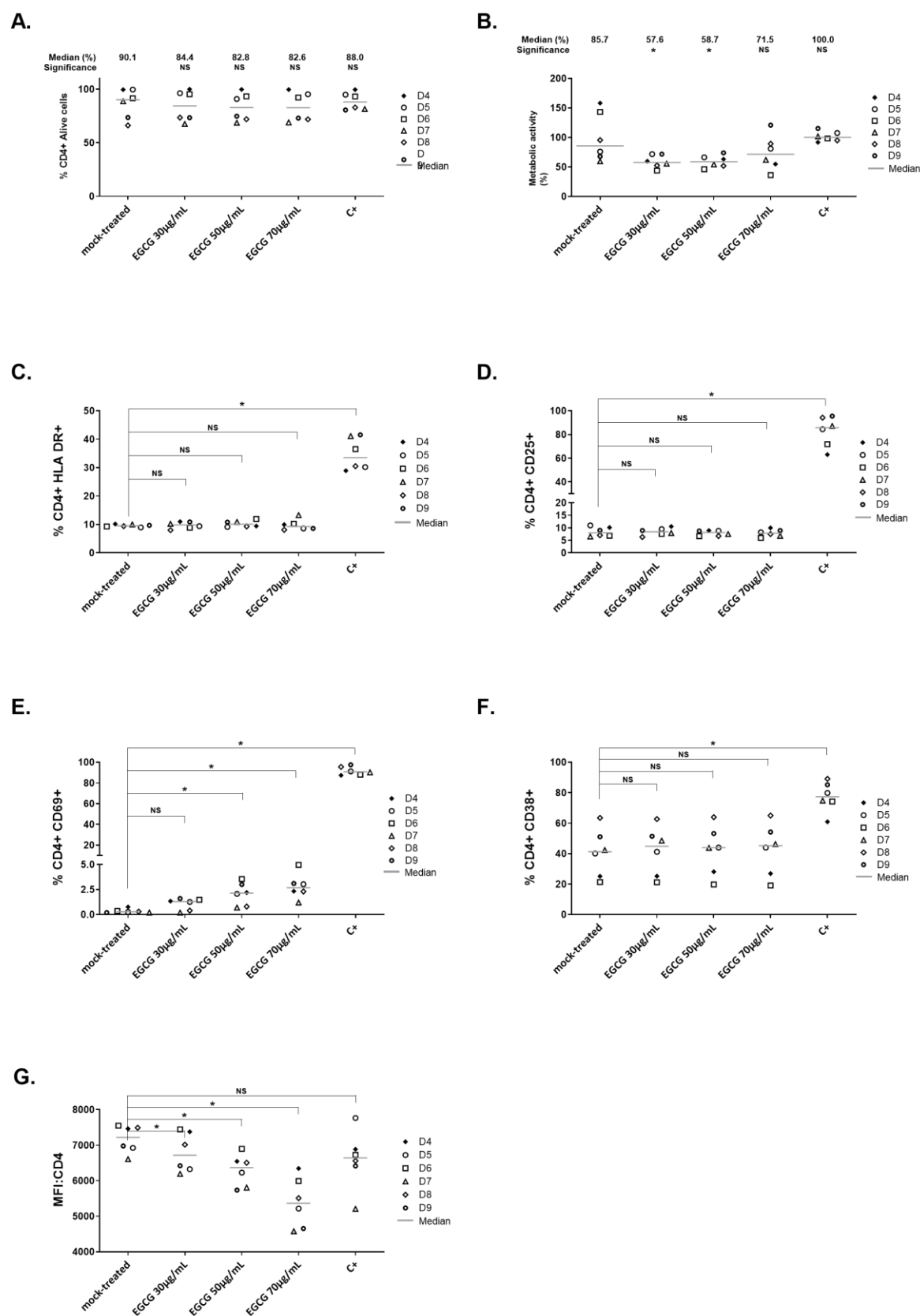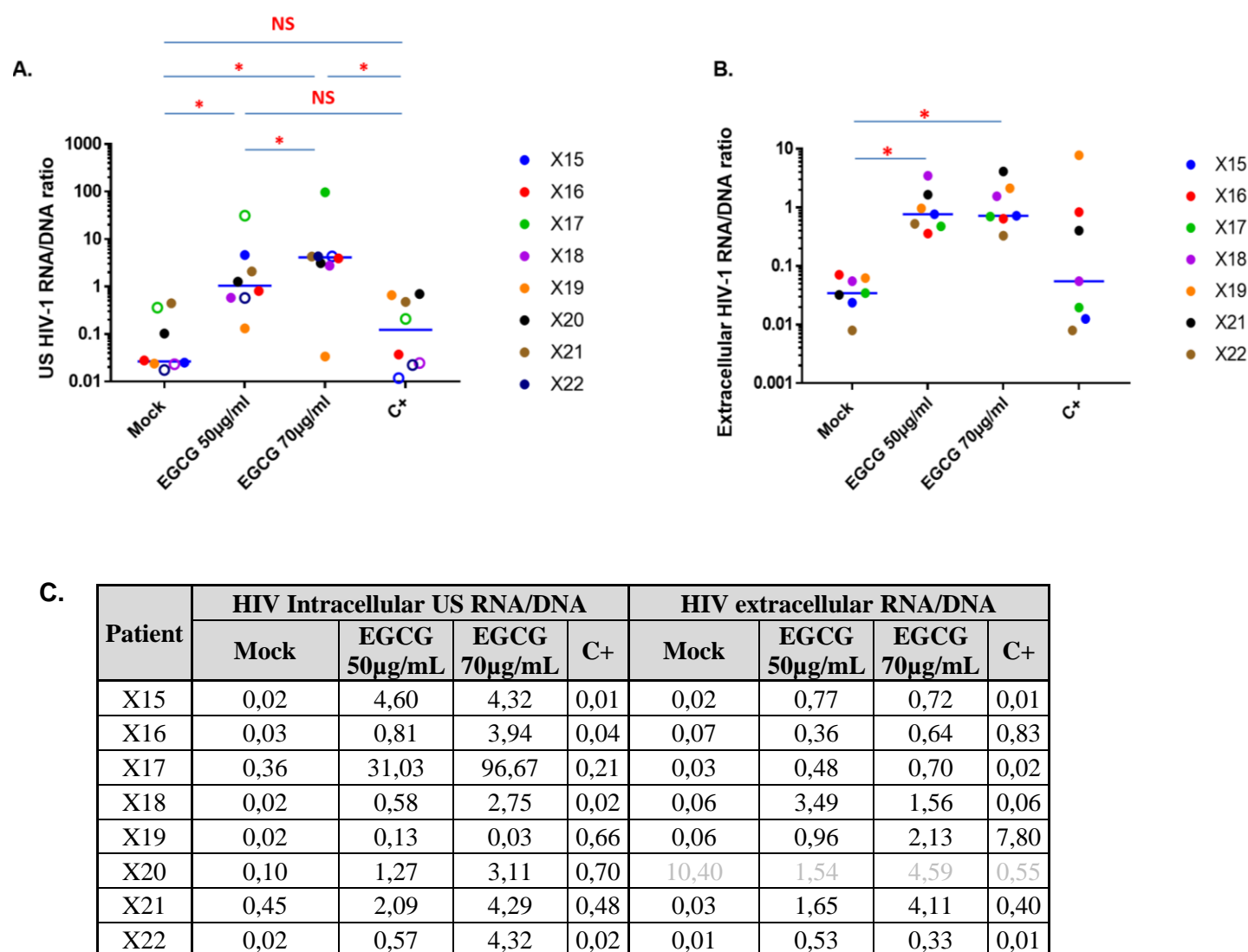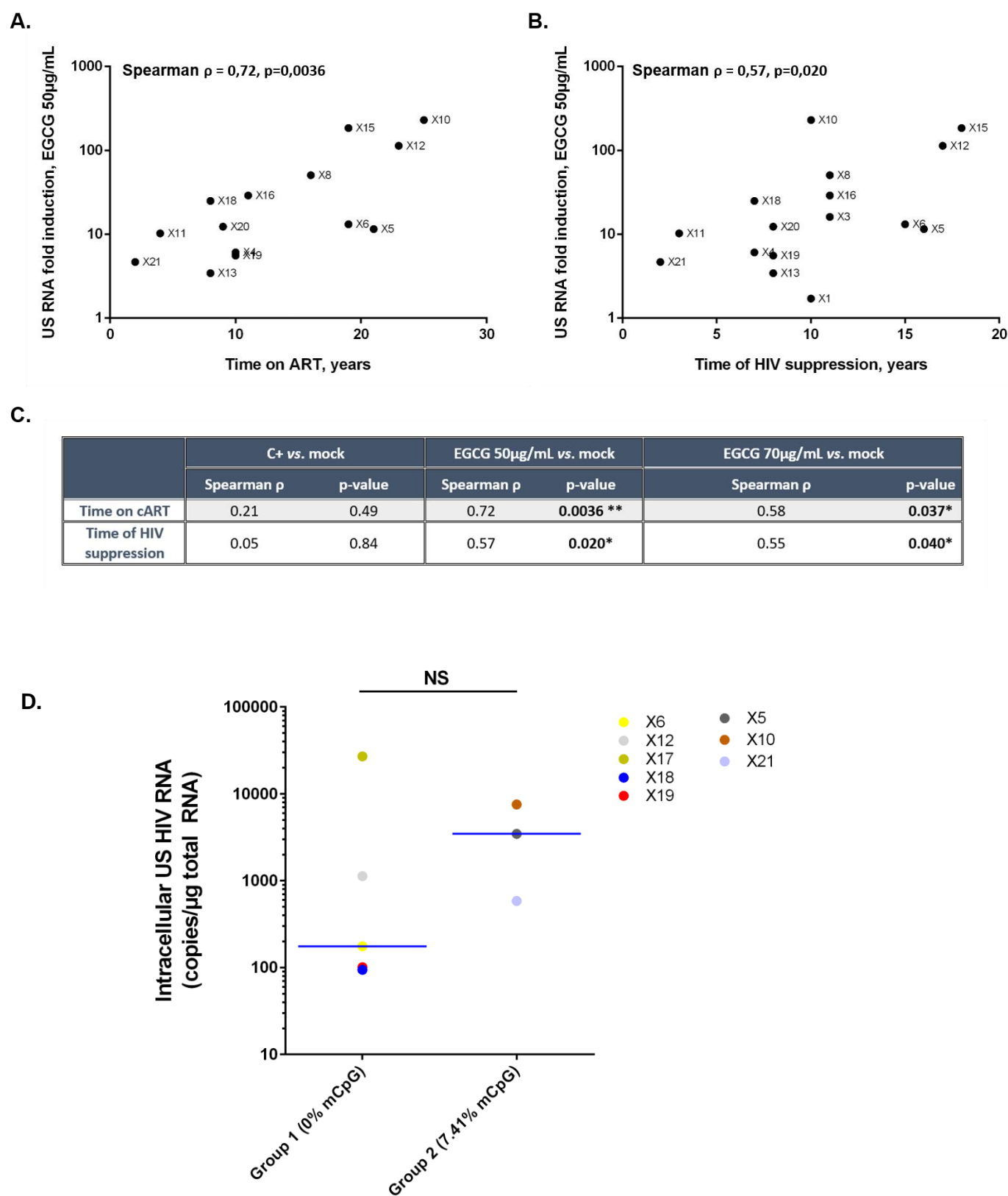| Cell type	Patient	Year of birth	Year of HIV diagnostic	HIV subtype	Race	CD4+ Nadir (cells/µL)	Year of 1st treatment	Year of undetectable status (<50 copies/ml)	Year of blood uptake	CD4+ T count at last point	Last treatment	Year of last treatment administration
CD8+-depleted PBMCs	X1	1952	?	?	Caucasian	315	?	2007	2017	636	RTV DRV	2012
	X2	1957	?	?	Caucasian	765	?	2015	2017	1221	STB	2015
	X3	1955	?	?	Caucasian	237	?	2006	2017	896	ART	2010
	X4	1978	2007	B	Caucasian	151	2007	2010	2017	561	GEN	2013
	X5	1964	1986	?	Caucasian	45	1996	2001	2017	598	KVX NPV	2002
	X6	1959	1998	B	Caucasian	215	1998	2002	2017	892	ART	2009
	X7	1963	2014	C	Afro-European	548	2015	2015	2017	684	TRI	2015
	X8	1939	2001	?	Caucasian	267	2001	2006	2017	1142	KVX EFV	2006
	X9	1966	1994	?	African	384	1997	1999	2017	871	RTV ATV EFV	2011
	X10	1957	1992	?	Caucasian	538	1992	2007	2017	598	TRU DTG	2016
	X11	1982	2013	B	Caucasian	379	2013	2014	2017	688	RPV DTG	2015
	X12	1939	1994	?	Caucasian	140	1994	2000	2017	650	KVX NPV	2015
	X13	1962	1995	?	African	286	2009	2009	2017	1304	GENVOYA	2016
	X14	1962	?	?	Caucasian	1011	?	2015	2017	1045	KVX RTV ATV	2009
	X15	1968	1996	?	African	225	1998	1999	2017	875	STB	2014
	X16	1969	2006	?	Caucasian	241	2006	2006	2017	893	KVX NVP	2014
	X17	1965	1996	?	African	280	1998	1998	2017	688	EVP	2017
	X18	1960	2008	?	Caucasian	307	2009	2010	2017	809	TRU EFV	2009
	X19	1949	2007	?	African	474	2007	2009	2017	574	KVX RTV DRV	2015
	X20	1949	2008	?	African	357	2008	2009	2017	606	KVX NVP	2014
	X21	1979	2015	B	Maghrebian	412	2015	2015	2017	963	GEN	2017
	X22	1943	1996	?	Caucasian	260	1997	1999	2017	782	EVP	2015

48

Patient	Total HIV-1 DNA (copies/10^6 PBMCs)	Log Total HIV-1 DNA (copies/10^6 PBMCs)	Intracellular US HIV RNA								Extracellular HIV RNA							
			24h stimulation				6 days stimulation				24h stimulation				6 days stimulation			
			Mock	EGCG 50μg/mL	EGCG 70μg/mL	C+	Mock	EGCG 50μg/mL	EGCG 70μg/mL	C+	Mock	EGCG 50μg/mL	EGCG 70μg/mL	C+	Mock	EGCG 50μg/mL	EGCG 70μg/mL	C+
X1	280	2.45	269	460	760	155	X	X	X	X	X	X	X	X	X	X	X	X
X2	653	2.82	17.9	744	4070	13.5	X	X	X	X	X	X	X	X	X	X	X	X
X3	2560	3.41	1060	17100	X	1990	X	X	X	X	X	X	X	X	X	X	X	X
X4	823	2.92	607	3690	X	428	X	X	X	X	X	X	X	X	X	X	X	X
X5	1517	3.18	299	3460	10200	1620	X	X	X	X	X	X	X	X	X	X	X	X
X6	740	2.87	13.3	176	995	22.1	X	X	X	X	X	X	X	X	X	X	X	X
X7	240	2.38	10.4	23.9	225	21.2	X	X	X	X	X	X	X	X	X	X	X	X
X8	943	2.97	277	14000	11200	353	X	X	X	X	X	X	X	X	X	X	X	X
X9	1650	3.22	9.11	671	X	319	X	X	X	X	X	X	X	X	X	X	X	X
X10	680	2.83	32.8	7550	X	508	X	X	X	X	X	X	X	X	X	X	X	X
X11	1210	3.08	24	247	X	52.9	X	X	X	X	X	X	X	X	X	X	X	X
X12	970	2.99	9.89	1130	12000	12	X	X	X	X	X	X	X	X	X	X	X	X
X13	4363	3.64	86	296	3690	946	X	X	X	X	X	X	X	X	X	X	X	X
X14	>13	>1.11	6.46	132	571	112	X	X	X	X	X	X	X	X	X	X	X	X
X15	717	2.86	17.9	3300	3100	8.48	6,75	X	X	957,55	1	551	516	I	1	176	244	24163
X16	1447	3.16	40.2	1170	5700	53.5	40,05	X	X	1185,47	103	520	931	1205	1	446	727	6438
X17	870	2.94	312	27000	84100	181	X	X	X	X	1	416	610	17	92	183	71	7074
X18	163	2.21	3.77	94.5	448	4.01	5,29	493,26	X	24,91	1	569	254	I	1	82	92	515
X19	767	2.88	18.2	101	25.8	507	160,95	1	X	508,90	1	740	1634	5979	411	658	X	7484
X20	347	2.54	35.7	441	1080	242	43,81	521,57	X	403,54	3608	534	1592	191	80	4127	750	1253
X21	280	2.45	125	585	1200	133	424,61	X	X	440,75	1	462	1151	113	105	644	328	11449
X22	1133	3.05	19.8	651	4900	25.3	23,64	X	X	438,97	1	596	373	I	1	217	1	2677

	Mock	EGCG 50μg/mL	EGCG 70μg/mL	C+	Mock	EGCG 50μg/mL	EGCG 70μg/mL	C+	Mock	EGCG 50μg/mL	EGCG 70μg/mL	C+	Mock	EGCG 50μg/mL	EGCG 70μg/mL	C+
# of activated patient cell cultures (over the limit of detection)	11	15	15	13	6	2	X	7	2	8	8	5	4	8	6	8
# of analyzed patient cell cultures	22	22	17	22	7	3	X	7	8	8	8	8	8	8	6	8
% of activated patient cell cultures	73.3	68.2	88.2	59.1	85.7	66.7	X	100	25	100	100	62.5	50	100	100	100